# Vanadium Dioxide for Energy Conservation and Energy Storage Applications: Synthesis and Performance Improvement

*Shancheng Wang,*[a] *Kwadwo Asare Owusu,*[c] *Liqiang Mai,*[*c] *Yujie Ke,*[a] *Yang Zhou,*[a] *Peng Hu,*[a] *Shlomo Magdassi,*[d] *and Yi Long*[*a, b]

a. *School of Materials Science and Engineering, Nanyang Technological University, 50 Nanyang Avenue, 639798 Singapore. E-mail:* longyi@ntu.edu.sg
b. *Singapore-HUJ Alliance for Research and Enterprise (SHARE), Nanomaterials for Energy and Energy-Water Nexus (NEW), Campus for Research Excellence and Technological Enterprise (CREATE), Singapore 138602*
c. *State Key Laboratory of Advanced Technology for Materials Synthesis and Processing, Wuhan University of Technology, Wuhan 430070, China. E-mail:* mlq518@whut.edu.cn
d. *Institute of Chemistry, Edmund Safra Campus, The Hebrew University, Jerusalem 91904, Israel*

KEYWORDS: Vanadium dioxide, Chemical vapor deposition, Atomic layer deposition, Smart-window, Lithium-ion battery, Supercapacitor

ABSTRACT: Vanadium dioxide ($VO_2$) is one of the most widely studied inorganic phase change material for energy storage and energy conservation applications. Monoclinic $VO_2$ [$VO_2$(M)] changes from semiconducting phase to metallic rutile phase at near room temperature and the resultant abrupt suppressed infrared transmittance at high temperature makes it a potential candidate for thermochromic smart window application to cut the air-condition usage. Meanwhile proper electrical potential, stable structure and good interaction with lithium ions make metastable $VO_2$ [$VO_2$(B)] an attractive material for fabrication of electrodes for batteries and supercapacitors. However, some long-standing issues have plagued its usage. In thermochromic application, high transition temperature ($\tau_c$), low luminous transmittance ($T_{lum}$) and undesirable solar modulation ability ($\Delta T_{sol}$) are the key problems, while in energy storage applications, short cycling lifetime and complex three-dimension microstructure are the major challenges. The common methods to produce $VO_2$ polymorph are physical vapour deposition (PVD), chemical vapour deposition (CVD), sol-gel synthesis, and hydrothermal method. CVD is an intensively studied method due to its ability to produce uniform films with precise stoichiometry, phase and morphology control. This paper reviews the various CVD techniques to produce $VO_2$ with controlled phases and the ternary

diagram shows the relationship between film stoichiometry and various process conditions. The difference between the various CVD systems are commented and the process window to produce $VO_2$ are tabulated. Some strategies to improve $VO_2$'s performance in both energy conservation and energy storage applications are discussed.

## Nomenclature

| | |
|---|---|
| AACVD | aerosol assisted chemical vapour deposition |
| ALD | atomic layer deposition |
| APCVD | atmospheric pressure chemical vapour deposition |
| AR-layer | anti-reflecting layer |
| CVD | chemical vapour deposition |
| CNT | carbon nanotube |
| DLI-MOCVD | direct liquid injection metal-organic chemical vapour deposition |
| FESEM | field emission scanning electron microscope |
| ITO | indium tin oxide |
| HVAC | heating, ventilation and air conditioning |
| MFC | mass flow controller |
| MIT | metal insulator transition |
| MOCVD | metal-organic chemical vapour deposition |
| PECVD | plasma enhanced chemical vapour deposition |
| PVD | physical vapour deposition |
| SEM | scanning electron microscope |
| SPR | surface plasmon resonance |
| $\tau_c$ | transition temperature |
| TEM | transmission electron microscope |
| TEMAV | tetrakis[ethylmethylamido]vanadium |
| $T_{lum}$ | luminous transmittance |
| VLS | vapour-liquid-solid |

$\triangle T_{sol}$   solar modulation ability

## Introduction

As the world population increasing, the energy demand of society increases rapidly. The world energy consumption in 2020 will increase to 53 billion kWh[1, 2]. Because of the limited amount of conventional energy sources such as coal, crude oil and natural gas, the current energy consumption practice has been proved as unsustainable. To fulfil the requirement of sustainability, approaches such as cutting off energy usage and exploring cleaner energy source have to be employed.

Energy saving in building is one of the important tasks in energy usage cutting off since building is one of the largest energy usage sectors. According to the report from United Nations, human-made building consumes 40% of total primary energy requirement globally and emits 30% of annual carbon dioxide emission[3]. Within the energy usage in building, heating, ventilation and air conditioning (HVAC) applications use about 50% of total energy[4]. Based on these data, reducing energy consumption for HVAC becomes an important task for architect and engineer. The HVAC energy consumption can be reduced via both aggressive and passive ways such as improving the efficiency of air conditioning system, adding thermal insulating to the wall, using cooling roof, and installing smart window glazing[5-7]. Since the window is the most energy inefficient component in the building, regulation the heat through the window becomes an important consideration for designer and national standard[8, 9]. Vanadium oxide ($VO_2$) is one of the phase change materials used as thermochromic smart window coating to cut off the energy consumption for regulating room temperature due to its near room temperature metal-insulator transition (MIT) and has attracted attention from academia and industry. When temperature increases above the transition temperature ($\tau_c$), the material transits from insulator to metal and its lattice changes from monoclinic to rutile with a diminished transmittance in the near-infrared range[10]. Therefore, temperature dependent solar modulation can be triggered automatically. Based on the heat reflection and absorption effect from the metallic state of $VO_2$, the building in warm-area (Cairo, Palermo and Rome) that employs $VO_2$ coated smart window shows an annual energy saving up to 10%[11]. Although $VO_2$(M) is attractive as an energy conservation material, some limitations restrict its application: First, bulk $VO_2$(M) has a $\tau_c$ at ~68°C, which is too high for room-temperature applications. Secondly, the integrated luminous transmission ($T_{lum}$) for $VO_2$(M) is only ~40% with a noticeable magnitude of solar modulation ($\Delta T_{sol}$) <20% which is insufficient for windows coating applications[12]. Nanothermochromism[13-15], controlled porous films[16], moth-eyed nanostructure[17], multi-layered antireflective over-coated films[18] and gridded structures[19-21] as shown in Figure 1 have been investigated to address those issues. The organic[22] and hybrid structure[23, 24] show superior $T_{\mathrm{lum}}$ and $\Delta T_{\mathrm{sol}}$, however they suffer from low durability and the translucent state at a high temperature, which is not favourable for window applications. In inorganic $VO_2$, the performance varies significantly due to the difficulty to control the crystallinity[25], uniformity, morphology[26] and phases because of its rich valence[27, 28].

On the other hand, although the cleaner energy such as solar energy and wind energy have been successfully commercialised, it is still very far from fully replacing the fossil fuel because of several limitations of the cleaner energy. For example, the photovoltaic panel can only generate electrical power during the daytime, and the amount of electricity generated by wind turbine is not stable since the speed of wind changes with time. Those issues prevent the large-scale application of solar and wind energy in everyday life[29]. Moreover, the development of electric vehicles based on the requirement to get rid of fossil fuel raises higher demand to the large capacity energy storage device [30]. Meanwhile, energy storage technology is also used to harvest the wasted kinetic energy from vehicle and large machine[31, 32]. Under this circumstance, metastable $VO_2$ [$VO_2$(B)] attracts attention in the energy storage area as battery and supercapacitor electrode materials and supercapacitor materials. $VO_2$(B) presents the advantage of having a proper electrode potential, which is desirable for batteries and supercapacitors[33]. Moreover, the unique tunnel structure of $VO_2$(B) allows lithium ion intercalate and deintercalate in reversible Li-ion battery[34]. Meanwhile, $VO_2$(B) has the outstanding resistance to the lattice shearing during charging cycling because of its increased edge shearing[35]. Lastly yet importantly, compared with the current cathode material in lithium battery such as $LiCoO_2$, the vanadium based cathode has lower cost due to the abundance in nature[36]. Since the morphology of electrode component has a significant influence on electrochemistry performance[37], a batch of one-dimension (1D) and two-dimensions (2D) structure such as nanorod[38], nanowire[39], nanobelt[40] and nanoparticles[41] have been produced. However, those structures suffer from poor cycling stability[42]. Three-dimensional (3D) microstructures such as flower-like structure[43], nanothorn hollow microsphere[42] and urchin-like structure[44] have been reported to exhibit superior cycling stability over 1D and 2D nanostructures because of the porous and rigid 3D structures. Meanwhile, several groups[45, 46] proved that carbon coating on electrode effectively improved electrode cycling stability. Despite the advances of these two ideas, there are still have some limitations. First, the thick carbon coating is not preferred in supercapacitor and battery electrodes as it hinders the diffusion kinetics of Li-ion and slows down the charge/discharge rate[47], which eliminates the advantage of tunnel structure in $VO_2$(B) crystal, Second, the current commonly used method such as hydrothermal process is not good at controlling film thickness precisely. Third, the complexity of the synthesis process for 3D microstructures and the difficulty in controlling the structure, stoichiometry and morphology also remain daunting tasks. Finally, current synthesis method is not suitable for large quantity production.

Compared with other fabrication methods such as physical vapour deposition (PVD)[48], sol-gel synthesis[13, 18, 21, 49], polymer-assisted deposition[50, 51], hydrothermal[52-54] and dip coating[55], CVD takes the advantages in producing high uniformity film with precise stoichiometric control on a large area. For example, a wafer-sized electronic-grade single crystalline $VO_2$ thin film fabricated with CVD has recently been produced by Zhang *et al.*[56]. Although the authors did not achieve mass production of $VO_2$, this case proved the capability of CVD to become an industrialised production technique. The objectives of this article are to review various CVD techniques used to deposit $VO_2$ thin film with controlled phases, to elaborate the processing parameters that affect the thin film quality and to discuss the strategies such as doping, forming of composite, ultra-thin overcoating and so forth (Figure 2), which can improve the performance of the films. The different phases, lattice, space group of $VO_2$ and their applications are shown in Table 1.

Table 1 Structures and some properties for four major phases of $VO_2$‡.

| Phase | Lattice | Space group | Application example | Remarks |
|---|---|---|---|---|
| $VO_2$(R)* | Tetragonal | $P4_2/mmm$ | Smart windows coating[57], High damping materials[58], Smart radiator devices for spacecraft[17], Field effect transistors[17], Resistive random-access memories (RRAMs)[59] | Stable from 68°C to 1540°C |
| $VO_2$(M) | Monoclinic | $P2_1/c$ | | Stable below 68°C |
| $VO_2$(A)† | Tetragonal | $P4_2/nmc$ | Unknown | Metastable |
| $VO_2$(B) | Monoclinic | $C2_1/m$ | Electrode, Supercapacitor | Metastable |

*$VO_2$(R) stands for the rutile phase of $VO_2$, which is produced by phase changing of $VO_2$(M) when the temperature above 68°C

†$VO_2$(A) is the intermediate phase in the phase transition from $VO_2$(B) to $VO_2$(R).

‡The lattice and space group information are summarised from Ref.[60].

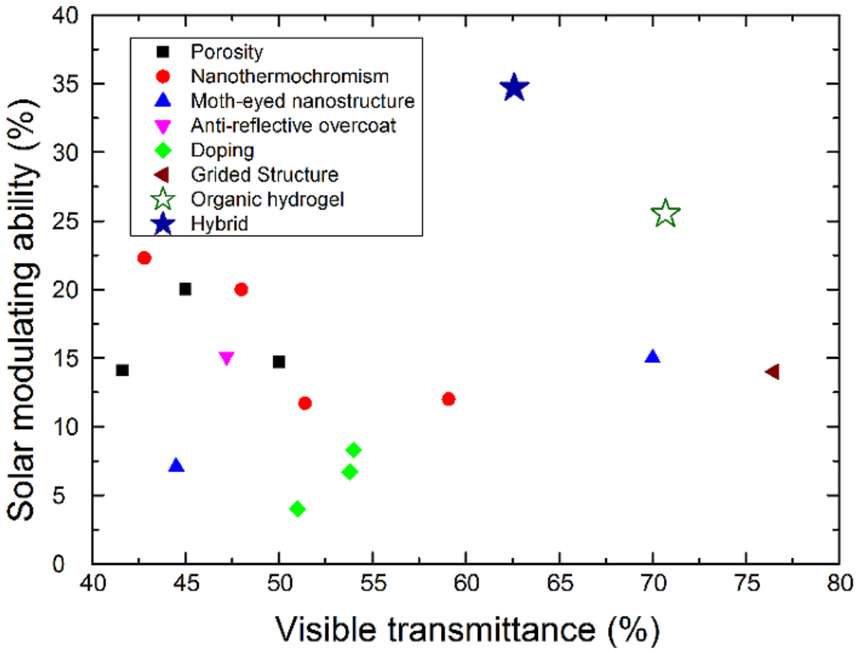

Figure 1 Thermochromic performance of film produced by the various methods. Adapted from Ref.[24] with permission from Wiley.

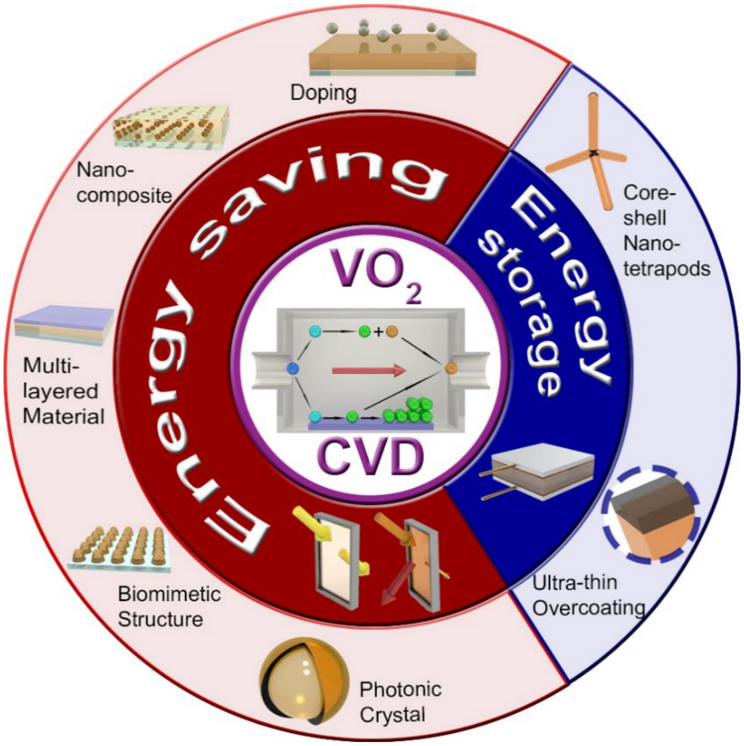

Figure 2 Strategies that enhance the performance of $VO_2$ for the energy saving and energy storage applications.

## 1. Chemical vapour deposition (CVD) of $VO_2$

CVD is a thin film deposition technique that is widely used in semiconductor and other industries. It utilises precursor vapour or gas precursor to react in a reaction chamber and deposits the product of reaction onto a substrate to form a thin film. The scheme of the entire process is presented in Figure 3. The precursors are first brought into the reaction chamber by the carrier gas (step 1) followed by the diffusion of the precursor from the main stream to the substrate, forming a boundary layer on the substrate surface (step 2a). In boundary layer, gas flow rate gradually decreases from main stream velocity to zero and the precursor is subsequently absorbed onto the substrate. Heterogeneous nucleation and reaction happen (step 3) with the film subsequently forming on substrates and coalescence (step 4). In contrast, in step 2b, homogeneous reaction may happen with powders produced above boundary layer and in most cases the film deposited with powders as crystallisation nuclei is not preferred due to poor adhesion and quality[61]. The by-products and unreacted precursor are transported out from the chamber at the end of the process (step 5a, 5b).

Depending on system configuration, there are several types of CVD system such as atmospheric pressure CVD (APCVD), plasma enhanced CVD (PECVD), metal-organic CVD (MOCVD) and so forth. These techniques to deposit $VO_2$ will be introduced in details later. The pros and cons of different CVD systems are summarised in Table 2.

Table 2 Advantages and disadvantages of some commonly used CVD techniques[62, 63].

| Type of CVD | Advantages | Disadvantages |
|---|---|---|
| APCVD | • Fast deposition rate<br>• Good robustness, easy to clean and maintain<br>• Simple system configuration | • Relatively low uniformity and step coverage<br>• Difficult to control film quality and volatile precursor is a must |
| PECVD | • Good film-substrate adhesion<br>• Able to deposit film at low temperature | • Plasma may damage substrate due to energetic particle bombardment<br>• Complex system configuration<br>• Difficult parameter controlling due to presence of plasma |
| MOCVD | • Able to control film thickness precisely<br>• Good film quality and uniformity | • Precursor is usually highly toxic<br>• High purity precursor is required<br>• Difficult to get rid of carbon contamination |
| AACVD | • Fast deposition rate<br>• Capable for non-volatile precursor | • Poor film-substrate adhesion<br>• Relatively high defect density |
| Hybrid AA/APCVD | • Suitable for composite production | • Complex system configuration<br>• Difficult to control synthesis parameters |
| ALD | • Precise thickness control<br>• Good uniformity<br>• Low defect density<br>• Able to deposit film at low temperature | • Slow deposition rate<br>• Complex system configuration |

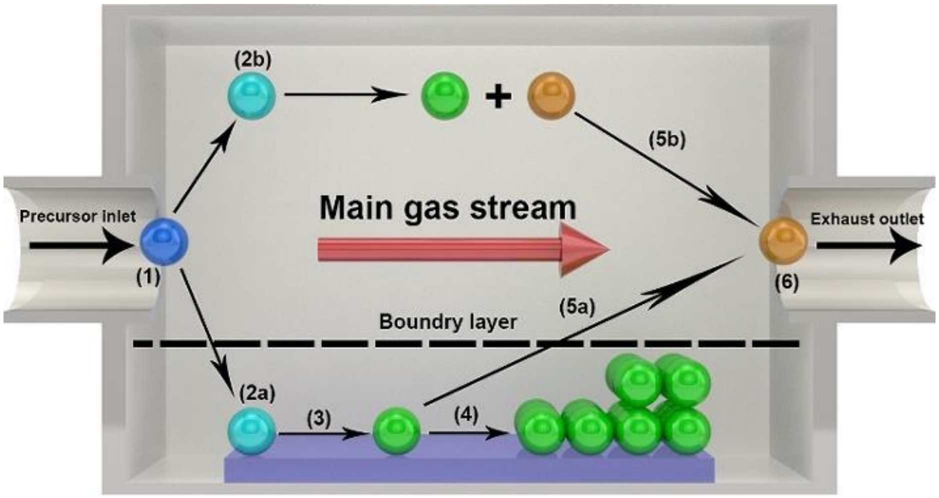

Figure 3 Schematic diagram of the CVD process: (1) precursor introduction; (2a) precursor absorbing; (2b) homogeneous reaction; (3) heterogeneous reaction; (4) film forming and coalescence; (5a), (5b) by-product transporting; (6) exhausting.

## 1.1. Atmospheric pressure chemical vapour deposition (APCVD)

APCVD is the CVD technique with atmospheric chamber pressure. The technique utilises inert gas such as argon or nitrogen to fill the chamber and maintain chamber pressure. A typical APCVD system configuration is shown in Figure 4, mass flow controller (MFC) is used to precisely control the flow rate of carrier gas. APCVD has a significant limitation: in order to produce sufficient precursor vapour, only volatile precursor can be used. The limitation restricts choosing of precursor, and sometimes bubbler has to be heated to ensure continuous vaporisation or sublimation of precursor.

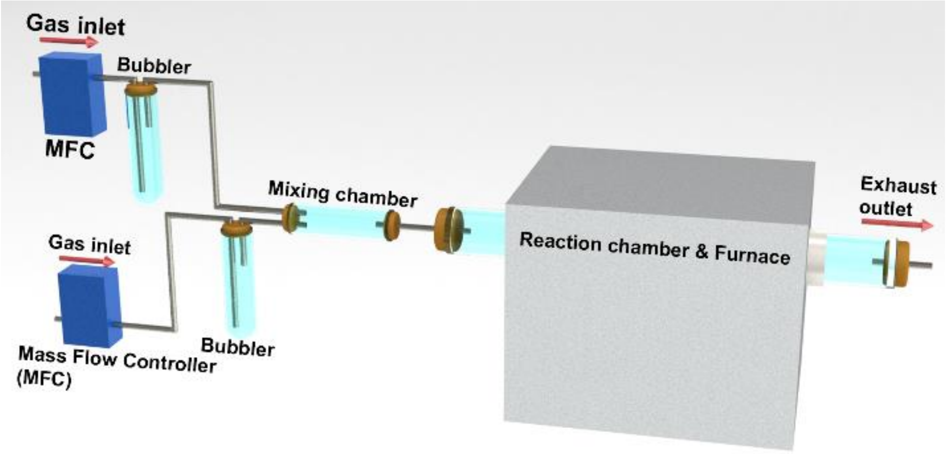

Figure 4 Schematic diagram for APCVD system.

Due to its simple system configuration, APCVD was applied to deposit $VO_2$ thin film from 1968[64]. In that experiment vanadium(V) oxytrichloride ($VOCl_3$) and carbon dioxide ($CO_2$)/carbon monoxide (CO) mixture gas were used as precursors. The transition temperature for deposited $VO_2$ film was 67°C, which was similar to $\tau_c$ of bulk $VO_2$. There are two types of precursors namely vanadium halide and vanadium-organometallic. In the vanadium halide system, two major precursors $VCl_4$ and $VOCl_3$ are used; while in the vanadium-organometallic system, $VO(acac)_2$ and $VO(OC_3H_7)_3$ are applied. The details are discussed separately in the following two sections.

### 1.1.1. Parameters that affect film growth in APCVD system with vanadium halide precursor

The phase diagram plotted by Kang[27] states that the two most critical factors for the composition of produced films is temperature and the ratio of mole fractions for V and O. As described in Figure 5, it should be noticed that the $VO_2$ pure phase can be produced at the oxygen mole fraction of 0.66 as marked by the arrow. With the oxygen mole fraction decreasing, triclinic Magnéli phases $V_nO_{2n-1}$ (n=4, 5, 6, 7, 8) will be formed. Hence, the reaction parameters must be carefully tuned to ensure the correct stoichiometry and phase.

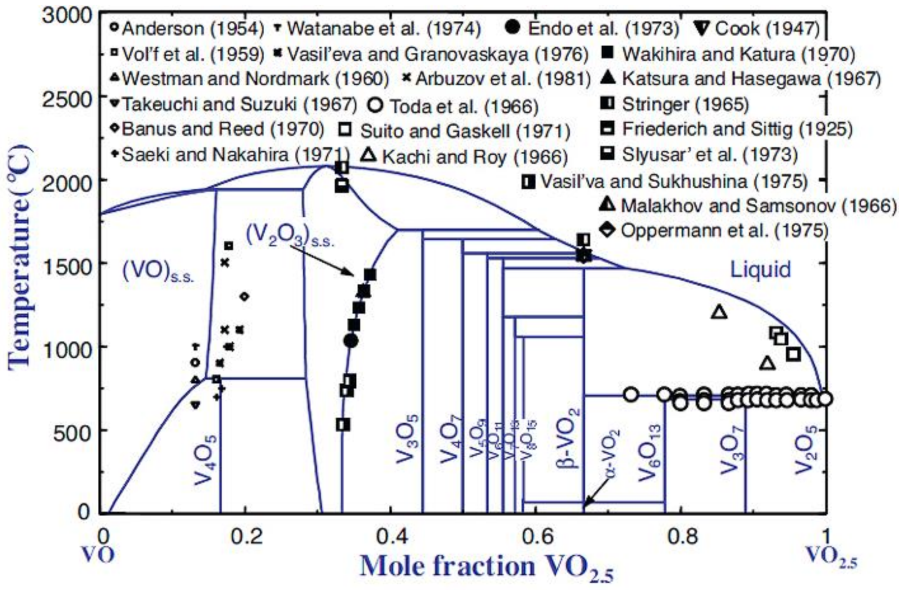

Figure 5 Phase diagram of $VO_x$ system. The arrows indicate the position of $V_2O_3$ and α-$VO_2$. The x-axis represents the mole fraction of $VO_{2.5}$ in the compound. For example, $V_2O_5$ is considered as $VO_{2.5}$; $VO_2$ can be regarded as the combination of **33%** of VO and **66%** of $VO_{2.5}$. α-$VO_2$ stands for $VO_2$(M), and β-$VO_2$ refers to $VO_2$(R). Reprinted from Ref.[27]. Copyright 2012, with permission from Elsevier.

Vernardou *et al.* conducted a series of experiments in 2006[65] and 2011[66] to show the effects of process parameters on the stoichiometry of film by using $VCl_4$ and $H_2O$ as the precursors with fixed flow rate of 12 L/min. In 2016, Gaskell *et al.* deposited $VO_2$(M) on fluorine doped tin oxide pre-coated borosilicate substrate by using the same precursor and fixed flow rate[67]. As summarised in Figure 6, it shows that when the substrate temperature was higher than 450 °C and $VCl_4$:$H_2O$ molar ratio was less than 0.5, $V_2O_5$, as marked in dark cyan region, was formed; while $V_2O_3$, as circled in purple, was formed when the $VCl_4$:$H_2O$ ratio was 1 and temperature was up to 450°C. In contrast, when the temperature was less than 400°C, in nearly all $VCl_4$:$H_2O$ ratio region except 0.6, there was no crystalline phase as shown in two olive rectangular boxes. The general trend suggested that with increasing $VCl_4$:$H_2O$ ratio, the valance of V of the produced decreased. Interestingly, $VO_2$, as marked in wine-coloured T shape zone, was able to be deposited on $SiO_2$ buffer layer pre-coated glass at 450-475°C with a $VCl_4$:$H_2O$ molar ratio of 0.55-0.8[65], however by changing different substrates, Gaskell could obtain $VO_2$ at lower temperature starting from 350°C by fixing the $VCl_4$:$H_2O$ molar ratio to 0.6[67]. The possible reason for this observation remains unknown.

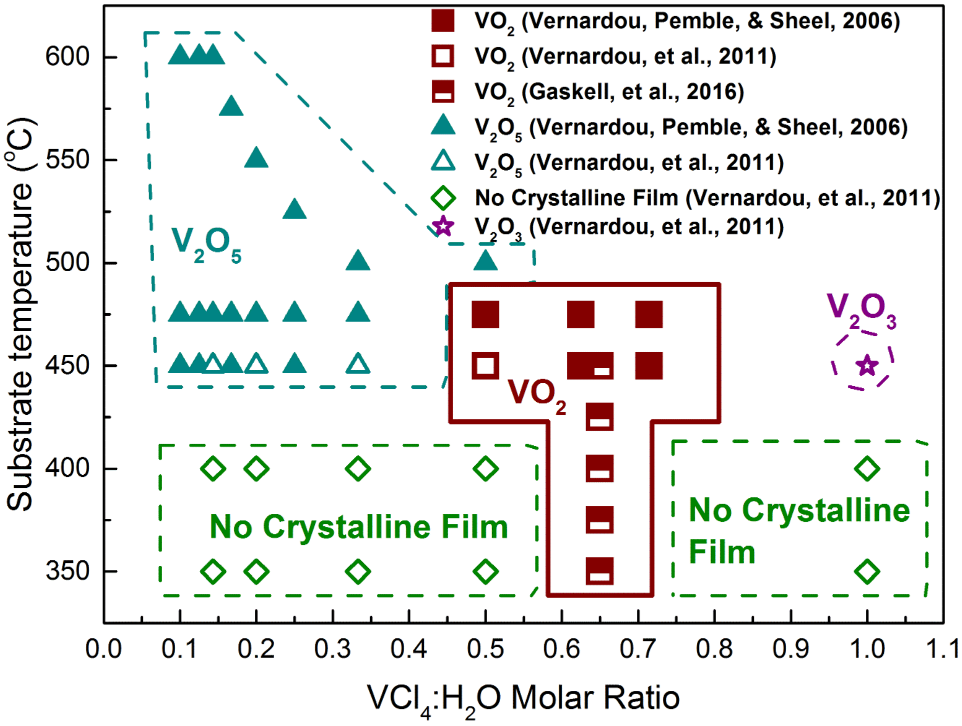

Figure 6 Binary diagram shows the results of Vernardou's[65, 66] and Gaskell's experiments[67].

It was found out the flow rate influences the phase formation of vanadium oxide. Figure 7 summarises the experimental results for both $VCl_4$-$H_2O$ and $VOCl_3$-$H_2O$ system including the effects of temperature, molar ratio and flow rate. Figure 7 (a) shows the ternary diagram indicating the relationship between film stoichiometry and variation of normalised parameters for both $VCl_4$ and $VOCl_3$ systems and Figure 7 (b) and (c) are the 3D-XYZ diagram of two different systems respectively for better viewing of the actual experimental conditions. From Figure 7 (a) and (b), we find that the $VO_2$ pure phase as shaded in wine-colour region could be deposited at two regions, namely region 1 at 350-475°C with a $VCl_4$:$H_2O$ molar ratio of 0.55-0.8 and a fixed flow rate of 12 L/min as well as region 2 at higher temperature (500-550°C), the richer $H_2O$ supply ($VCl_4$:$H_2O$ molar ratio from 0.05 to 0.2) and a slower flow rate (~1 L/min). It is worth noting that by adding dopants such as Ti and W, the process condition varied. Specifically, titanium-doped $VO_2$ was formed with significantly high flow rate (18 L/min), which can be obviously observed in Figure 7 (b). By increasing substrate temperature and the fraction of V-precursor, $V_2O_5$ could be formed with flow rate fixed at 12 L/min with an exception when the flow rate reduced dramatically to ~ 1.5 L/min and decreased temperature from 450 to 475°C as shown in Figure 7 (b). In the lower flow region, $V_6O_{13}$, as shaded in navy blue, could be formed with increased $VCl_4$ concentration compared with $V_2O_5$.

The use of $VOCl_3$ as a precursor is relatively rare in recent years. By combining Figure 7 (a) and (c), it shows that $VOCl_3$-$H_2O$ system produced $V_2O_5$ and $V_2O_5$-$V_6O_{13}$ mixing phase at the temperature 350-600°C with the $VOCl_3$:$H_2O$ molar ratio from 0.6 to 4 and the flow rate of 1.5-3.5 L/min. The $V_2O_5$ production region for the $VOCl_3$-$H_2O$ system in Figure 7 (a) was larger than the region of the $VCl_4$-$H_2O$ system which suggests that $V_2O_5$ is more readily formed with this precursor. However, no $VO_2$ pure phase production was observed. The parameters and results differences between $VCl_4$-$H_2O$ and $VOCl_3$-$H_2O$ system can be explained by the different reaction mechanism. The reaction happened in $VCl_4$-$H_2O$ system is a simple hydrolysis reaction. In contrast, a reduction-oxidation (redox) reaction happens in $VOCl_3$-$H_2O$ system. Therefore, the $VCl_4$ system is easier to control than the $VOCl_3$ system and recommended for $VO_2$ growth.

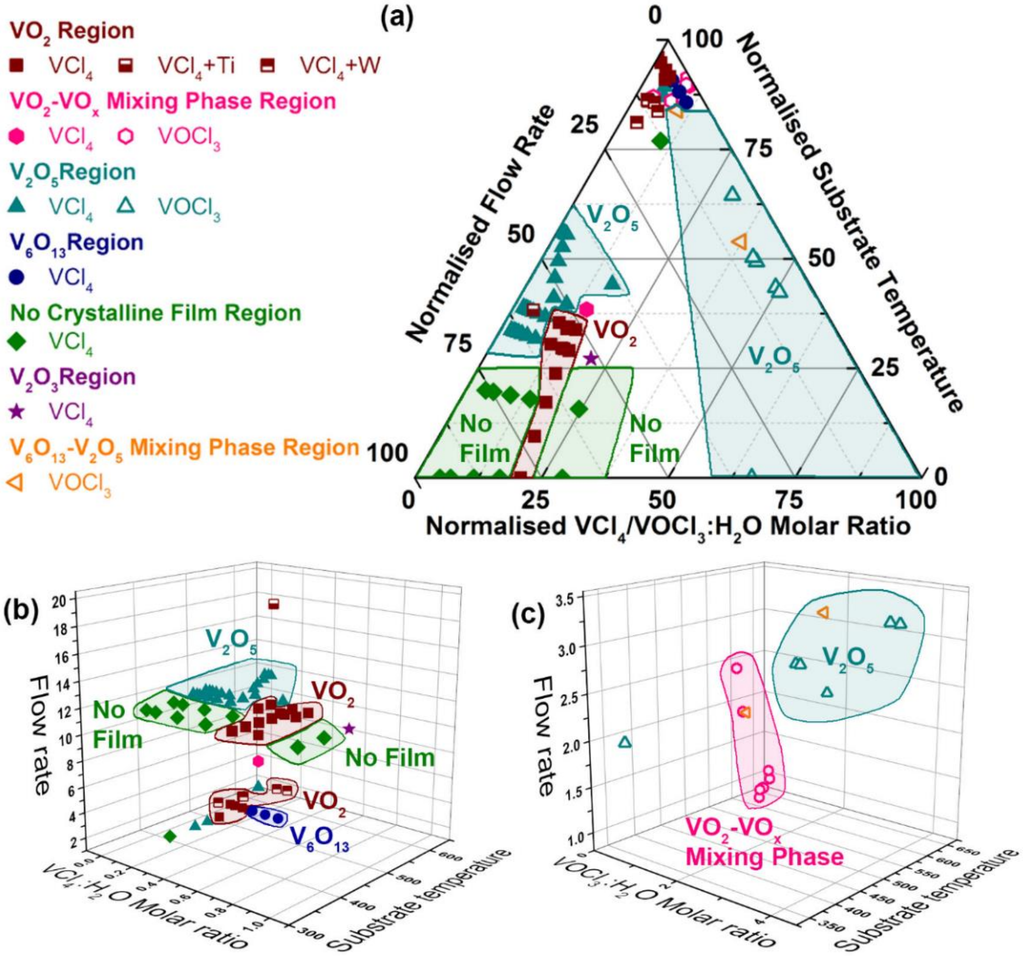

Figure 7 (a) Ternary diagram shows the relationship between film stoichiometry and variation of normalised parameters in both $VCl_4$ and $VOCl_3$ systems. (b) 3D-XYZ diagram shows the experiment results for $VCl_4$ systems. (c) 3D-XYZ diagram shows the experiment results for $VOCl_3$ system. The data of $VCl_4$ system are collected from Ref.[65-70]. The data of $VOCl_3$ system are collected from Ref.[71].

### 1.1.2. Parameters that affect film growth in APCVD system with vanadium-organometallic precursor

Similar to the system with vanadium halide, the film stoichiometry in the vanadium-organometallic applied system is affected by temperature, the molar fraction of the precursor, and total flow rate. Vernardou *et al.* evaluated the influence of variations in conditions on the stoichiometry in the system with $VO(acac)_2$ and oxygen and plotted a binary diagram[65]. As described in Figure 8, the deposition for $VO(acac)_2$ required a higher temperature compared with the $VCl_4$ system as explained in section 1.1.1 and the process window was much wider regarding oxygen flow rate

(0.1-0.9 L/min). In $VO(acac)_2$ system, the intramolecular decomposition is the major reaction, while the reaction between $VCl_4$ and $H_2O$ is a simpler intermolecular hydrolysis reaction.

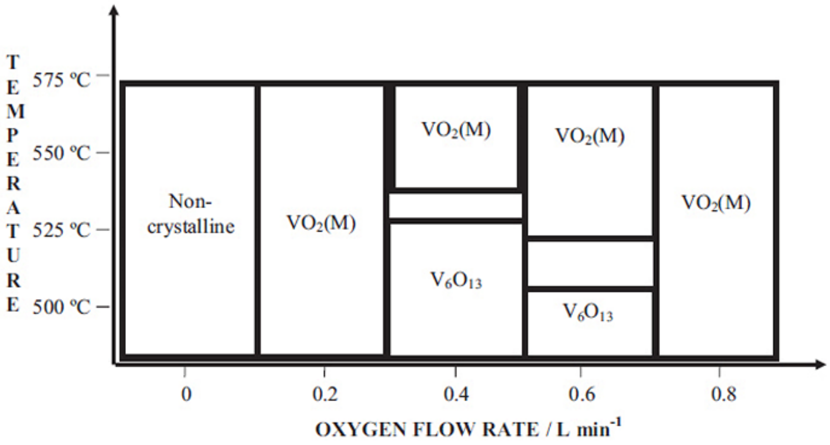

Figure 8 Influence of oxygen flow rate and temperature on film stoichiometry at a fixed total flow rate of 12L/min in APCVD. Reproduced from Ref.[65] with permission from Wiley.

There are several publications[72-75], which reported successful deposition with $VO(OC_3H_7)_3$ on $SnO_2$ pre-coated glass, and indium tin oxide (ITO) coated substrate. The growth temperature of these experiments was set in the range of 300-450°C, which was significantly lower than the optimum growth temperature for $VO(acac)_2$ system (Figure 8). In two reports[73, 75] the stoichiometry of film produced with different carrier gas flow rate through precursor was particularly evaluated. The results showed that in the temperature range of 400-450°C, $VO_2$ could produce with the $O_2$ flow rate in the range of 2-4 L/min.

Similar to halide precursor system, deposition of $VO_2$ film with vanadium-organometallic was affected by different substrates such as borosilicate glass, fused quartz, (1 0 0) MgO single crystal, (1 0 0) $SrTiO_3$ crystal, (1 0 0) Si wafer, and randomly oriented sapphire [72, 74, 76]. It has been found that the pure $VO_2$ was deposited only on fused quartz and sapphire substrate while mixture phases of $V_3O_7$ or $V_4O_9$ were formed on other substrates. The difference among substrates could be due to the lattice mismatch and thermal coefficient expansion of $VO_2$ and substrates.

## 1.2. Metal-organic chemical vapour deposition (MOCVD)

The pressure of MOCVD system varies from 1 torr to atmospheric and two categories of precursors are commonly used: (1) β-diketonates such as $VO(acac)_2$, $V(acac)_3$ and vanadyl bis-hexafluoro acetylacetonate [$VO(hfa)_2$] and (2) alkoxides such as $VO(OC_3H_7)_3$ and vanadyl ethoxide [$VO(OC_2H_5)_3$][77]. However, the performance of these precursors is different. Barreca *et al.* evaluated performances of four kinds of β-diketonates precursors: $VO(acac)_2$, $VO(dpm)_2$, $VO(fod)_2$ and $VO(hfa)_2(H_2O)$ (Note: Hdpm: 2,2-6,6-tetra-methyl-3,5-heptanedione; Hfod:2,2-dimethyl-6,6,7,7,8,8,8-hepta-fluoro-3,5-octanedione) [78]. The first three precursors produced $VO_2$ in oxygen atmosphere while the last one only produced $V_2O_5$ in oxygen but could produce $VO_2$ in a nitrogen atmosphere.

The precursor applied in MOCVD can be in vapour or liquid form. The direct liquid injection MOCVD (DLI-MOCVD) can control film stoichiometry more precisely[79].

### 1.2.1. Parameters that affect film growth in MOCVD

The film stoichiometry in MOCVD is affected by temperature and the molar fraction of precursor[65] and the molar fraction in MOCVD system is mainly controlled by oxygen flow rate. As shown in Figure 9, the optimum growth temperature for DLI-MOCVD was 375-475°C, which was significantly lower than for APCVD (Figure 8) but DLI-MOCVD seemed to have narrow process window. When the oxygen flow rate was between 0.02 and 0.04 L/min, $VO_2$(M) single phase was produced at the temperature in the range of 450-475°C. Furthermore, when the oxygen flow rate was within 0.04 to 0.08 L/min, $VO_2$(M) and $VO_2$(B) mixed phase would be deposited at 425°C. However, if the temperature decreased to 400°C, $VO_2$(B) single phase would be produced.

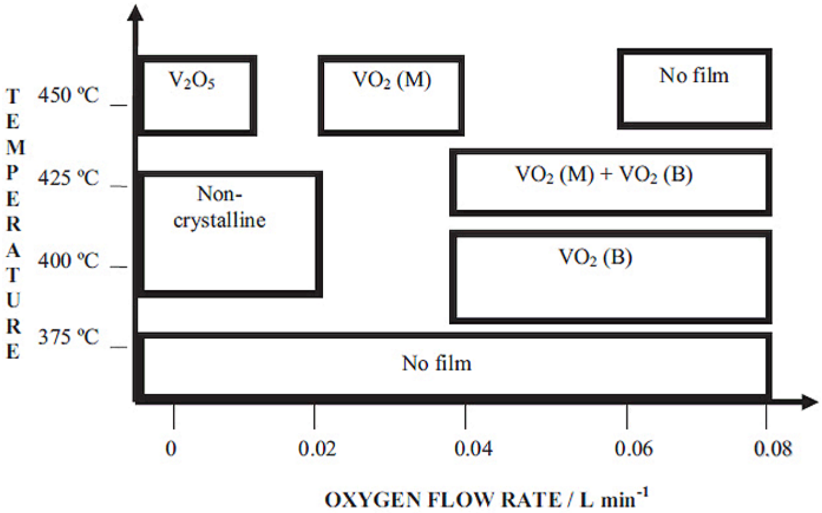

Figure 9 Influence of oxygen flow rate and temperature on film stoichiometry at a fixed total flow rate of 3 ml/h in a MOCVD system. Reproduced from Ref.[65] with permission from Wiley.

Spanò *et al.* studied the influence of growth temperature (200 to 750°C) on the film morphology and stoichiometry in a 3 torr MOCVD reactor with an oxygen flow rate of 0.15 L/min as shown in Figure 10[77]. $VO_2$ was produced at 200-350°C, which was lower than Vernardou's experiment (Figure 9)[65]. During the experiment, when the temperature increased to 400-500°C, $V_6O_{13}$ was formed. Moreover, $V_2O_5$ deposition was observed if the temperature was higher than 500°C. The structure of film growth at 200°C consisted nanocolumns with the width of 70-80 nm [Figure 10 (a)]. If temperature increased to 300°C, the plate-like structure appeared and the width kept increasing with increasing temperature [Figure 10 (b)-(f)][77].

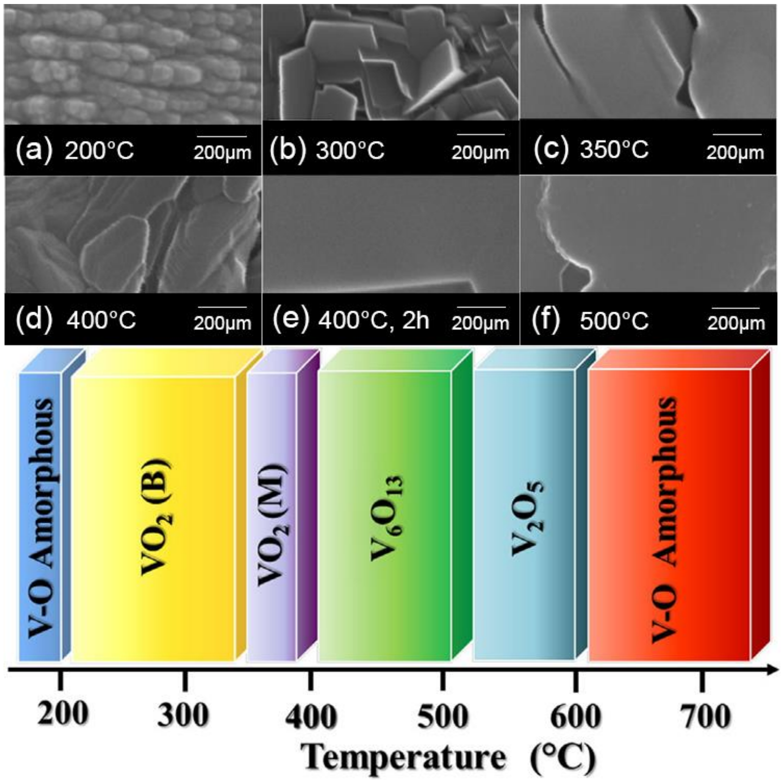

Figure 10 Morphologies and compositions of film produced at different growth temperatures with MOCVD. Adapted from Ref.[77] with permission from Wiley.

## 1.3. Plasma enhanced chemical vapour deposition (PECVD)

PECVD has an advantage in thin film deposition compared to the other deposition techniques, as it utilises either a strong electrical field or microwave to produce plasma to decompose precursor and promote film formation which results in lower temperature deposition. However, there are rare reports of $VO_2$ synthesis with PECVD due to the complexity of the PECVD system. Interestingly, several groups have reported the synthesis of $V_2O_5$ with vanadium organometallic precursor and oxygen gas [80-82]. The synthesis of $V_2O_5$ is relatively easy because $V_2O_5$ is the most thermodynamically stable phase at room temperature. In 1998, Zhang *et al.* produced vanadium oxide for battery cathode, using $VOCl_3$, $O_2$ and $H_2$ as precursors [83]. The radio-frequency power was used to form the plasma with $V_6O_{13}$ thin film produced, which gave a high discharge capacity of 408 mAh $g^{-1}$, negligible capacity fading after repeated charging and energy density of 960.3 Wh $kg^{-1}$. The chemical reactions involved in the synthesis of $V_6O_{13}$ are: $4VOCl_3 + 6H_2 + 3O_2 \leftrightarrow 2V_2O_5 + 12HCl$ and $12VOCl_3 + 18H_2 + 7O_2 \leftrightarrow 2V_6O_{13} + 36HCl$. A similar idea can be used to synthesize $VO_2$. Since vanadium atoms in $VO_2$ has a valence number of +4, Zhang's experiment can be modified by selecting precursors with vanadium valence number of +4 or reducing the amount of oxygen so that $VO_2$ could be produced. Therefore, we recommend employing precursors such as $VCl_4$ and $VO(acac)_2$ to avoid the possible introduction of an oxidant or reductant.

## 1.4. Aerosol assisted chemical vapour deposition (AACVD)

AACVD utilises aerosol instead of vapour to produce thin film. Commonly, an ultrasonic humidifier (Figure 11) is used to generate a precursor aerosol which circumvents the limitation of volatile precursor allowed in APCVD. The aerosol is firstly transported into the reaction chamber as shown in Figure 11 with the solvent evaporated and remaining precursor particles absorbed onto the substrate followed by heterogeneous reaction. The film is deposited on the substrate, and by-products are desorbed and transferred away from substrate[84].

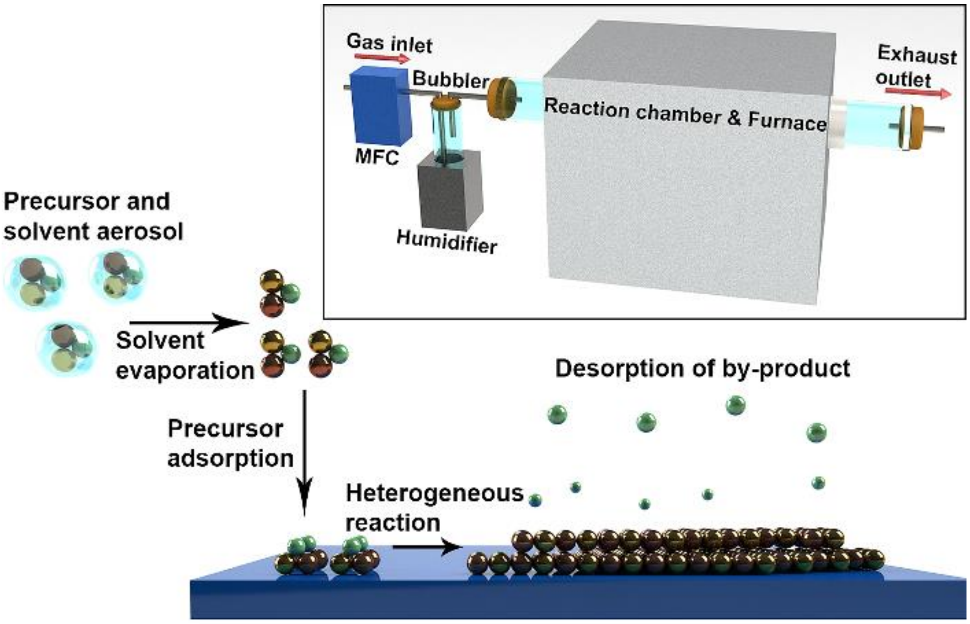

Figure 11 Mechanism and system configuration for AACVD.

Naik *et al.* produced $VO_2$ pure phase with $VO(acac)_2$ single precursor via AACVD[85]. The precursor was dissolved in ethanol and formed aerosol by an ultrasonic humidifier. Nitrogen gas served as carrier gas in the experiment. The $VO_2$ pure phase was produced at 450-600°C with an island growth morphology. Besides $VO(acac)_{2,}$ commonly used precursors for AACVD includes $V(acac)_3$[86] and other kinds of organic metal oxide.

The effects of external electrical field to the morphology of $VO_2$ film were extensively researched[87-92]. The applying of electrical field decreased the average particle size, increase the film porosity, enlarge the surface area but more prone to oxidation[93].

AACVD has some limitations such as poor adhesion between film and substrate, and relatively high defect density[61]. Those limitations might be due to the rapid deposition speed. Since a large number of the particles are deposited on the substrate in short time, they do not have enough time to diffuse and re-arrange themselves to the lower energy growth site.

## 1.5. Hybrid AA/APCVD

Hybrid AA/APCVD combines the systems and advantages of both AACVD and APCVD as shown in Figure 12. This system can deposit film with high quality and uniformity. At the same time, it can add nanoparticle into film by using nanoparticle slurry aerosol. Hybrid CVD method is suitable for producing nanocomposite.

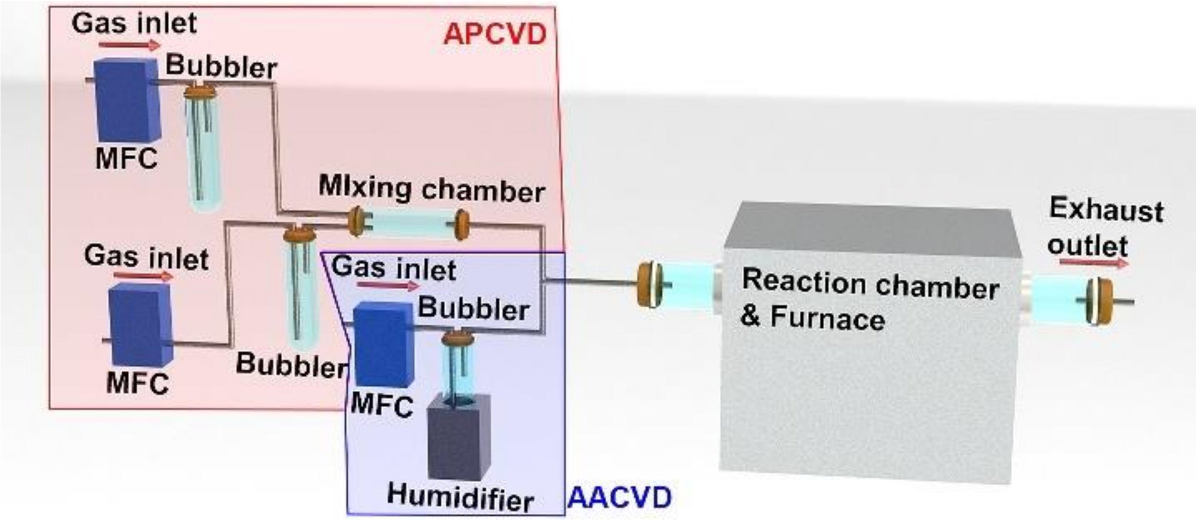

Figure 12 Schematic diagram for hybrid AP/AACVD.

Warwick *et al.* produced the plain $VO_2$ thin film, $VO_2$-$TiO_2$ nanocomposite and $VO_2$-$CeO_2$ nanocomposite by hybrid CVD (Figure 13)[94]. The $VO_2$ film was synthesised with $VO(acac)_2$ and oxygen. $VO(acac)_2$ was heated in the bubbler and carried by nitrogen-oxygen mixture gas into the reaction chamber. At the same time, nanoparticles were transported into the chamber in the form of aerosol. All the composites showed reduced $\tau_c$ compared with bulk $VO_2$, and the reflectance showed a significant change of 30% between at 25°C and 80°C. The films had the photocatalytic properties similar to titanium dioxide thin film. The group concluded that although the $T_{lum}$ of the nanocomposite was still needed to be improved, hybrid CVD is a promising way to produce thermochromic nanocomposite.

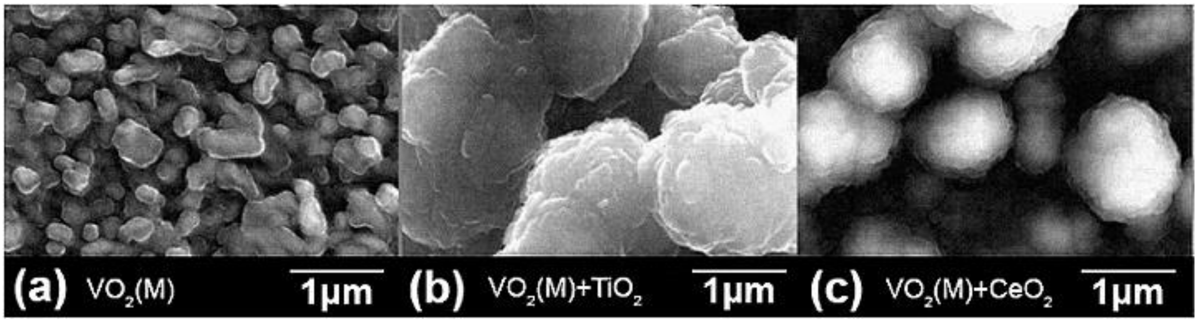

Figure 13 Scanning electron microscope (SEM) image for (a) plain $VO_2$ thin film, (b) $VO_2$-$TiO_2$ nanocomposite and (c) $VO_2$-$CeO_2$ nanocomposite. Reprinted from Ref.[94]. Copyright 2011, with permission from Elsevier.

## 1.6. Atomic layer deposition (ALD)

ALD is an "extreme" case of CVD. It utilises self-terminating surface half-reactions to control deposition. Since only a single molecular layer is formed in one cycle, ALD can form a very high-quality thin film with precise thickness control. The reaction cycle must be repeated for several times to deposit thicker film, which makes ALD a slow and high-cost CVD technique. Tetrakis[ethylmethylamido]vanadium (TEMAV) is the vanadium contained precursor commonly used in ALD[95-99]. Other precursors used in ALD include $VO(OC_3H_7)_3$[100] and $VO(acac)_2$[101]. The common oxygen source used in ALD includes water[100], ozone[99, 102] and oxygen plasma[103].

The self-terminating surface half-reaction is the foundation of ALD process. Factors such as reaction temperature, precursor injection time and purging time have to be carefully tuned in order to achieve this reaction. To form a saturated monolayer, the binding energy between substrate and precursor should be larger than the binding energy between the monolayer and precursor particles above[104]. Therefore, a precise temperature controlling is required. As the amount of injected precursor has to be in excess to ensure that a saturated layer is formed, an adequate purging time is needed for the excess precursor to evacuate the reaction chamber. The report of Rampelberg *et al.* demonstrated a typical ALD process for $VO_2$(M) film deposition at 150°C with TEMAV and $O_3$ as precursors as shown in Figure 14[99]. Firstly, TEMAV was introduced into the system to form multilayers followed by purging and re-evaporation of excess precursors to ensure the monolayer formation. $O_3$ was introduced into the system and reacted with TEMAV; the unreacted $O_3$ was purged out of the chamber. An amorphous $VO_2$ film was produced and then was subsequently annealed at 450°C in a He atmosphere for 30 min to form $VO_2$(M) phase.

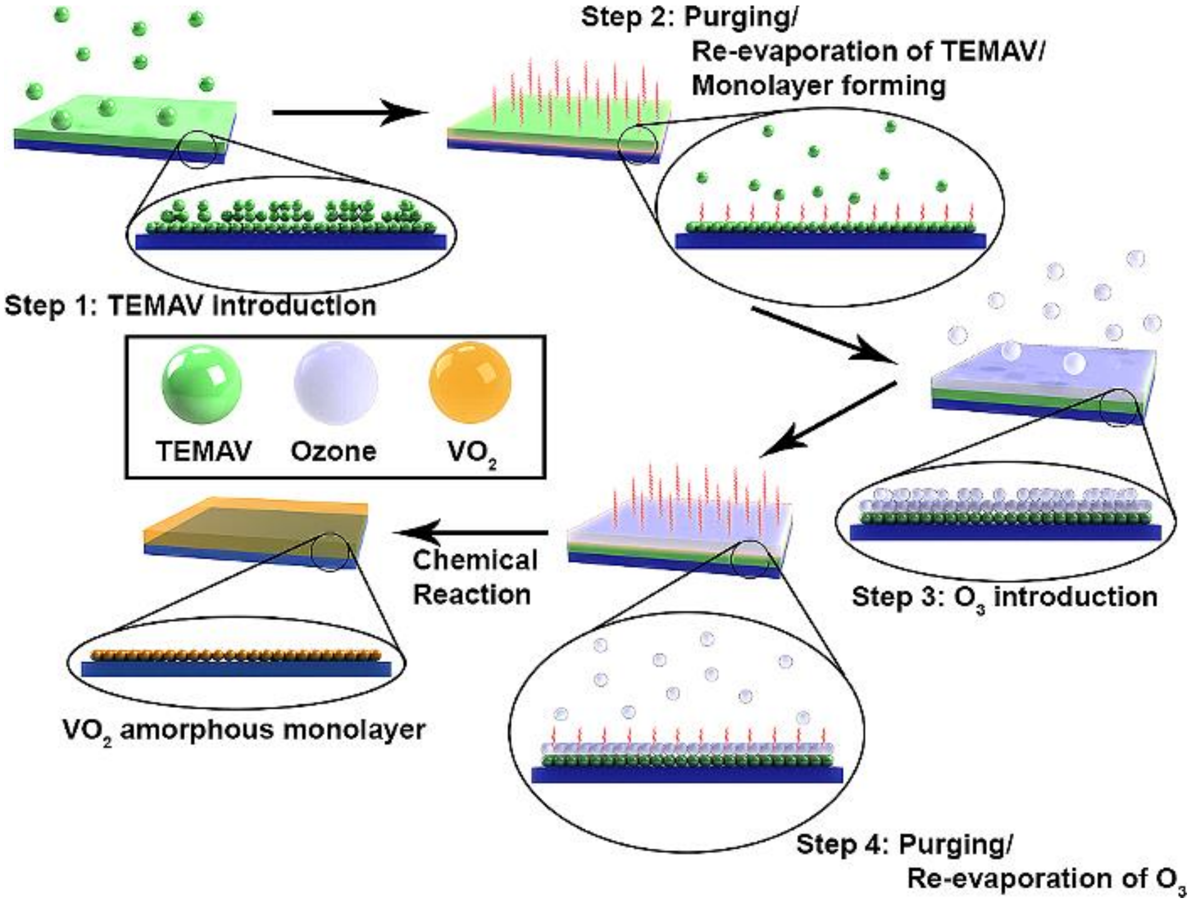

Figure 14 Schematic diagram showing the ALD process reported in Rampelberg *et al*.[99]'s case.

The parameters of different CVD to produce $VO_2$ is summarised in Table 3. It can be seen that vanadium-organometallic precursors such as $VO(acac)_2$ and $VO(OC_3H_7)_3$ have the largest process window for APCVD, MOCVD and AACVD system, which are especially suitable for the system with rough condition controlling. $VCl_4$-$H_2O$ system can deposit pure phase $VO_2$ with little contamination but because of its high toxic and narrow process window, it highly recommends establishing an APCVD system with good sealing and precise condition controlling when applying this precursor. TEMAV is the precursor with the lowest reaction temperature. Although currently it is only used for ALD, the precursor has high potential to be used in other CVD techniques such as MOCVD and AACVD. The least used precursor $VOCl_3$ is not recommended because of the difficulty to produce $VO_2$ pure phase and the highest reaction temperature among precursors.

Table 3 Precursor and parameters for various CVD techniques to deposit pure phase $VO_2$(M), pure phase $VO_2$(B), mixture of $VO_2$(M) and $VO_2$(B) and $VO_2$-$VO_x$ mixing phase.

| Method | Precursor/ Results | Controlling | | | Remarks |
|---|---|---|---|---|---|
| APCVD | $VCl_4$-$O_2$† | Molar ratio | T (°C)‡ | Flow rate (L/min) | • Able to produce pure $VO_2$ phase with little contamination<br>• Recommend for the system with precise condition controlling. |
| | | 0.45-0.8 | 350-475 | 12 | |
| | | 0.05-0.2 | 500-550 | 0.5-1 | |
| | $VOCl_3$-$O_2$/Mixing phase | 0.5-1 | 600-650 | 0.5-2.5 | • Produce mixing-phase only<br>• Not recommended. |
| | | $O_2$ Flow rate (L/min) | T (°C) | Total flow rate (L/min) | • Wide process window<br>• Recommend for the system with rough condition controlling<br>• Have potential carbon contamination, which may affect optical properties. |
| | VO(acac)$_2$-$O_2$/ $VO_2$(M) | 0.1-0.9 | 475-575 | 12 | |
| | VO($OC_3H_7$)$_3$-$O_2$/ $VO_2$(M) | 0.6 | 300-450 | 0.7-0.8 | |
| | | Precursor flow rate (L/min) | T (°C) | Total flow rate (L/min) | • Able to produce $VO_2$ film with the single precursor<br>• Suitable for the application with low purity requirement<br>• Relatively simple system configuration. |
| | VO($OC_3H_7$)$_3$/ $VO_2$(M) | 2-4 | 400-450 | 12 | |

| | | | | | | |
|---|---|---|---|---|---|---|
| | | P (torr) | T (°C) | Injection rate | $O_2$ flow rate (L/min) | |
| MOCVD | VO(acac)$_2$-$O_2$/ $VO_2$(M) | 760 | 430-475 | 3 ml/h | 0.02-0.04 | • Wide process window<br>• Able to control reaction conditions more precisely than APCVD |
| | | 3 | 300-350 | 0.15 L/min | 0.15 | |
| | VO(acac)$_2$-$O_2$/ $VO_2$(M)+$VO_2$ (B) | 760 | 410-430 | 3 ml/h | 0.04-0.08 | |
| | VO(acac)$_2$-$O_2$/ $VO_2$(B) | 760 | 380-430 | 3 ml/h | 0.04-0.08 | |
| | | 3 | 200-300 | 0.15 L/min | 0.15 | |
| | | Solvent | | T (°C) | Flow rate (L/min) | |
| AACVD | VO(acac)$_2$/$VO_2$(M) | Ethanol | | 450-600 | 1.5 | • High deposition rate but relatively poor quality<br>• Suitable for the applications with low film quality requirement. |
| | V(ACAC)$_3$/ Mixing phase | Ethanol | | 500-600 | 1.5 | |
| | | P (torr) | | T (°C) | Pulse plan (s) * | |
| ALD | TEMAV-$O_3$/ $VO_2$(M) | $7.5 \times 10^{-7}$ | | 150 | 2-25-5-15 | • Precise control of film thickness but complex system<br>• Suitable for the application with high requirement to film thickness.<br>• TEMAV is especially suitable for application requires low process temperature. |
| | VO(acac)$_2$-$O_2$/ $VO_2$(M) | 10 | | 400-475 | 4-2-1-1 | |

‡"T" stands for growth temperature; "P" stands for chamber pressure.

†Due to the lack of phase information in some of the reference, we cannot differentiate the optimum conditions for $VO_2$(M) and $VO_2$(B) in $VCl_4$-$H_2O$ system.

*Pulse plan describes the purging step in ALD. The four values indicate the time for metal precursor injection, first purging, oxygen/ozone injection and second purging.

# 2. Strategies used in CVD system for improving $VO_2$ film's energy conservation performance

## 2.1. Doping

$VO_2$ application in thermochromic smart window is limited by high $\tau_c$ and doping is the effective way to reduce $\tau_c$. We summarised the effect of various dopants on the thermochromic performance in Table 4. Only a few elements have been doped using CVD, including W, F, Mo and Nb. Tungsten is an extensively used dopant for $VO_2$ due to its effectiveness in reducing $\tau_c$[105]. Commonly used W-contained precursors include $WCl_6$[106-108], $W(OC_2H_5)_6$[107] and $W(OC_2H_5)_5$[109, 110]. As the Table 4 and Figure 15 (c) describe, W has the most outstanding effect of $\tau_c$ decreasing among the dopants and the $\tau_c$ decreasing effect is linearly related to the W concentration. Despite the effectiveness of decreasing $\tau_c$, W doping has the shortcomings to reduce $T_{lum}$ and $\Delta T_{sol}$.

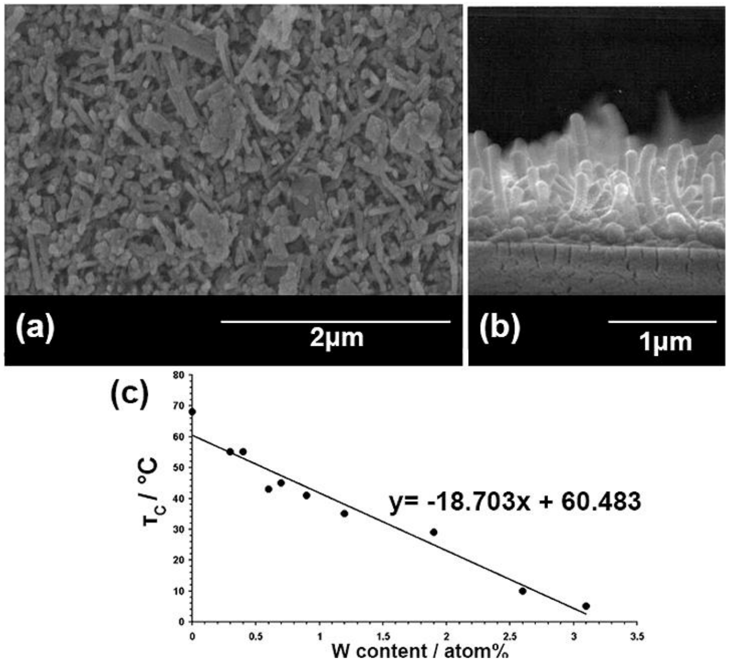

Figure 15 SEM image from (a). top down and (b) cross-section view of $V_{0.988}W_{0.012}O_2$ film produced by APCVD showing the worm-like structure. (c) Plotted relationship between W concentration and measured $\tau_C$ in the experiment. Adapted from Ref.[107] with permission from The Royal Society of Chemistry.

Other dopants such as Mo, Nb and F encountered the same problem (Table 4): They can only improve either one or two properties of $VO_2$. For example, Nb decreased $\tau_c$, $T_{lum}$ and $\Delta T_{sol}$ at the same time[111]. F could only increase $T_{lum}$ but broaden the hysteresis loop width at the same time[112, 113]. Although Mo was able to decrease $\tau_c$ and increase $T_{lum}$ at the same time, the reduction of Mo ion during CVD limited the effect of performance optimising[114].

Table 4 Effect of dopants on the thermochromic performance of $VO_2$ films.

| Dopant | $\tau_{c}$* | $T_{lum}$ | $\Delta T_{sol}$ |
|---|---|---|---|
| $W^{6+}$ **[105, 115, 116]** | ↓ (~20-26°C per at%) | ↓ | ↓ |
| $Ti^{4+}$ **[117, 118]** | ↑ | ↑ | ↑ |
| $Co^{2+}$ **[119]** | ↓ | n.a. | n.a. |
| $Ta^{5+}$ **[119]** | ↓ | n.a. | n.a. |
| $Nb^{5+}$ **[111, 120, 121]** | ↓ (~2°C per at%) | ↓ | ↓ |
| $Mo^{6+}$ **[120, 121]** | ↓ (~3°C per at%) | ↑ | ↓ |
| $Cr^{3+}$ **[122]** | ↑ | ↑ | ↓ |
| $Sn^{4+}$ **[123]** | ↑ (~1°C per at%) | n.a. | n.a. |
| $Al^{3+}$ **[124]** | ↓ (~2.7°C per at%) | n.a. | n.a. |
| $Fe^{3+}$ **[125]** | ↓ (~6°C per at%) | n.a. | n.a. |
| $Ce^{3+}$ **[126]** | ↓ (~4.5°C per at%) | n.a. | n.a. |
| $P^{3-}$ **[127]** | ↓ | n.a. | n.a. |
| $Sb^{3+}$ **[128]** | ↓ | ↑ | n.a. |
| $Tb^{3+}$ **[129]** | ↓ | ↑ | ↑ |
| $La^{3+}$ **[130]** | ↓ (~1.1°C per at%) | ↑ | ↑ |
| $Eu^{3+}$ **[131]** | ↓ (~5°C per at%) | ↑ | ↑ |
| $Mg^{2+}$ **[14, 132-134]** | ↓ (~3°C per at%) | ↑ | ↑ |
| $Zr^{4+}$ **[135]** | ↓ (~0.4°C per at%) | ↑ | ↑ |

In the table, "↑" and "↓" stand for the positive and negative effect on the properties respectively and "n.a." stands for data not available.

*The data in the brackets stand for the decreasing of $\tau_c$ per at% of dopant adding.

Two remedies namely discovering new dopants and co-doping were employed to meet the challenge of decreasing $\tau_c$ and increasing $T_{lum}$ and $\Delta T_{sol}$ at the same time. Several new dopants such Mg, Zr and rare earth elements like Eu, Tb and La can reduce $\tau_c$, enhance $T_{lum}$ and $\Delta T_{sol}$ at the same time (Table 4). It is worthwhile to employ CVD to dope such elements in future as CVD is a gas phase process which can facilitate the doping effectiveness.

On the other hand, co-doping is a more time-saving strategy since it improves $VO_2$ properties by combining the strength of currently available dopants and avoids their shortcomings. Some groups reported promising performance improvement by W/F co-doping[115] and W/Mg co-doping[119] and rare-earth/W co-doping[136]. The W/Mg co-doped sample prepared by Wang *et al.* via dip coating with $V_2O_5$, $H_2O_2$, Mg and W powder showed a decreased $\tau_c$ (~35°C) and an outstandingly high $T_{lum}$ (81.3%) which was one of the highest $T_{lum}$ among the reported cases[119]. Since CVD is a method that especially suitable to produce doped uniform thin film due to its mechanism and system configuration, co-doping is a future research topic with high potential and application value for CVD.

## 2.2. Forming of composite materials

CVD is suitable to produce certain types of composite materials: AACVD and hybrid AP/AACVD are good at producing nanocomposite and mixing phase materials since they can distribute nanoparticles and different phases in the matrix evenly. Conventional APCVD, MOCVD and ALD are more suitable to produce multi-layered structure materials and template assisted growth of biomimetic and photonic structure due to their ability to deposit high-quality thin film.

Gold/$VO_2$ nanocomposite is the most intensively studied form of nanocomposites due to the surface plasmon resonance (SPR) of gold nanoparticles and the changing of optical performance introduced by SPR[137]. Several groups reported the preparation of gold/$VO_2$ nanocomposite with $HAuCl_4$ as (gold) Au provider via hybrid AP/AACVD, the observation of a film colour changing (from a brown colour to blue-green colour)[109] and $\tau_c$ decreasing (~42°C)[138]. The influence of SPR to the optical and thermochromic properties of $VO_2$ requires future detailed investigate. Since the size and shape of nanoparticle can directly affect the SPR effect, the formation of nanocomposite with different particle size and shape, nanocomposite performance characterisation and structure optimising are attractive topic to research. Furthermore, because other precious metal such as Ag also has SPR effect, the nanocomposite between $VO_2$ and other precious metals and its performance is an interesting topic to be discovered.

Mixing phase is a reliable way to prepare multi-functional materials. Some groups produced multi-functional material that combined the photocatalytic properties from $TiO_2$ and thermochromic properties from $VO_2$ via APCVD or hybrid AP/AACVD with $TiCl_4$[69, 139] or $Ti(O^iPr)_4$[140]. All samples in those cases showed a decreased $\tau_c$ at ~50°C with a promising photocatalytic effect.

Multi-layer structure is an effective way to produce high-performance or multifunctional materials. Liu *et al.* produced $VO_2$ thin film with enhanced $T_{lum}$ and $\Delta T_{sol}$, promising hydrophobicity and anti-oxidation ability by coating a Si-Al based anti-reflecting layer (AR-layer) via sol-gel method[18]. Meanwhile, Evans *et al.* prepared $TiO_2$/$VO_2$ multilayer samples with different structures ($TiO_2$ on

$VO_2$ and $VO_2$ on $TiO_2$) and observed that the morphology of both composites was dominated by $TiO_2$ (Figure 16) [141]. Moreover, the $TiO_2$ on $VO_2$ sample showed the thermochromic and photocatalytic properties from both $VO_2$ and $TiO_2$ but the sample of $VO_2$ on $TiO_2$ did not show any photocatalytic effect and $\tau_c$ decreasing. Recently, Breckenfeld *et al*. partially explained the reason behind this phenomenon [142]. As reported by the researchers, the thermochromic properties of $VO_2$ on $TiO_2$ is affected by the epitaxial strain due to the lattice mismatch between these two crystals. Epitaxial strain helps to reduce the $\tau_c$ by introducing lattice instability. However, if the $VO_2$ layer is too thick, misfit dislocations will occur and relax the accumulated epitaxial strain. The group proposed a way to solve this problem: carefully choosing the crystal growth direction of both $TiO_2$ and $VO_2$, and then annealing the composite to inhibit the generation of misfit dislocation. CVD (especially MOCVD) is good at growing the crystal with certain growth direction. Moreover, unlike other methods such as PLD, sputtering and solution based method, it is possible to anneal the sample without taking it out of the chamber using CVD, which prevents the sample from potential contamination and protects the good quality of the sample.

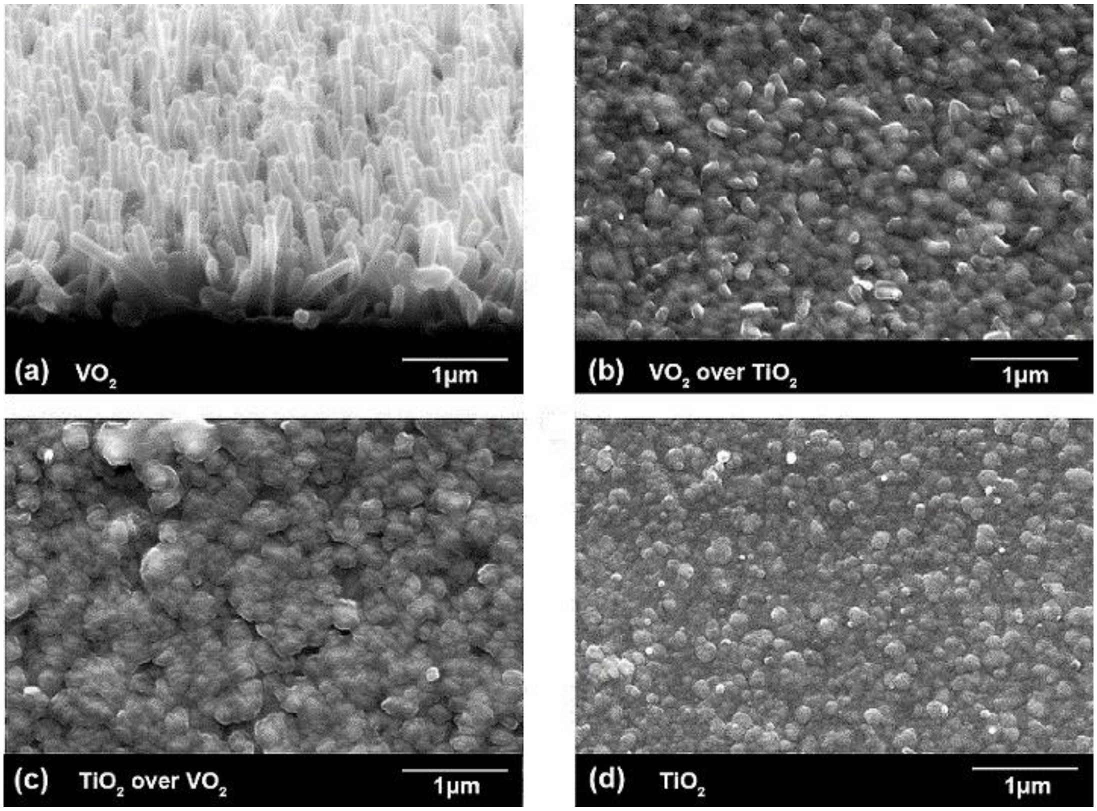

Figure 16 SEM images of a). VO$_2$; b). VO$_2$ on TiO$_2$; c). TiO$_2$ on VO$_2$; d). TiO$_2$. Two composites had morphologies that were similar to TiO$_2$. Reprinted from Ref.[141]. Copyright 2007 with permission from Elsevier.

## 2.3. Template-assisted growth

Biomimetic structures enhance the thermochromic performance of VO$_2$ film since the sub-wavelength moth-eye structures provide a continuous refractive index gradient between the air and the medium, which effectively decreases the reflections by reducing the refractive index gap on the air-medium interface. The simulation conducted by Taylor *et al.*[143] [Figure 17 (a)-(c)] and the sample prepared by Qian *et al.*[17] via templated assisted sol-gel method [Figure 17 (d)-(h)] confirmed the ability of biomimetic structures to enhance $T_{\mathrm{lum}}$ and $\Delta T_{\mathrm{sol}}$ as showed in Figure 17 (i) and (j). Compared with the sol-gel method, CVD especially APCVD and MOCVD have the advantage to deposit high quality and uniformity film on the complex geometry surface. Therefore, producing the biomimetic structure via CVD and its performance evaluation is an attractive future research topic.

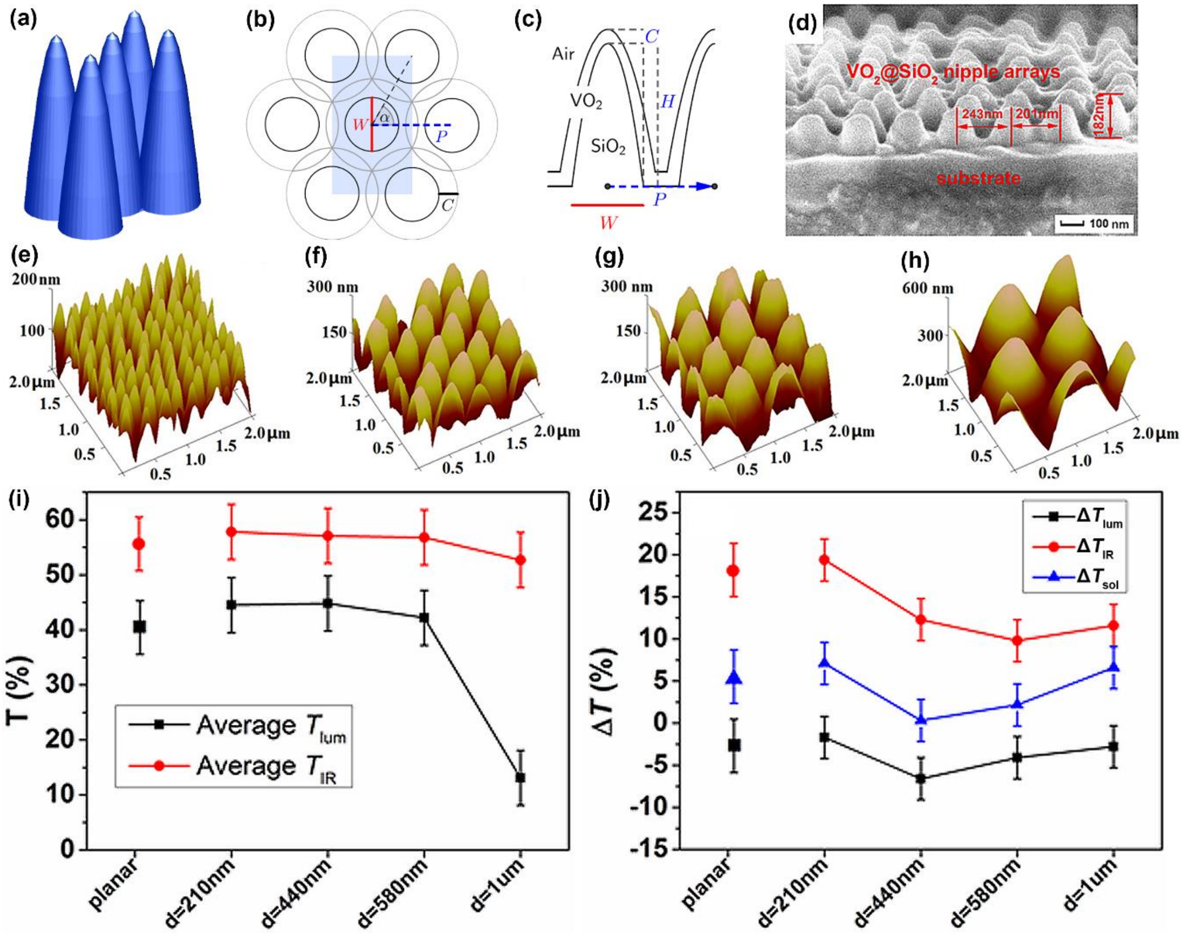

Figure 17 (a) 3D illustration of nanotextured surface with nipple arrays. (b) Side and (c) top views of hexagonally arranged circular paraboloid cones. (d) SEM cross-sectional profile of the moth-eye nanostructured $VO_2$ film. AFM analyses of the biomimetic $VO_2$ films with varied moth-eye structure size of (e) 210, (f) 440, (g) 580, and (h) 1000 nm. Effects of the moth-eye structure size on (i) $\Delta T_{lum}$, $\Delta T_{IR}$, and $\Delta T_{sol}$ as well as on (j) $T_{lum}$ and $T_{IR}$. (a)-(c) are adapted from Ref. [143] with permission. Copyright 2013 The Optical Society. (d)-(j) are adapted from Ref.[17] with permission. Copyright 2014 American Chemical Society.

Photonic crystal is one of the promising structures to display conspicuous structural colour due to its photonic bandgap generated by coherent optical diffraction. Ke *et al.* produced two-dimensional $SiO_2$-$VO_2$ core-shell thermochromic photonic sphere via template-assisted sol-gel process[Figure 18 (a)][55]. The simulation results [Figure 18 (b)] and the experiment results [Figure 18 (c)] both indicated that such structure could achieve both diameter-dependent colours and reliable thermochromic performance. However, because the sol-gel method was not good at preparing high uniformity film with good complex geometry coverage, the actual $T_{lum}$ and $\Delta T_{sol}$ was slightly derivate from the simulated values. CVD as a technique that good at producing coating with good coverage can solve the issue encountered in Ke’s experiment. Recently, Ke *et al.* applied the same method to produced various nanopatterns[144], which also provided ideas for energy saving applications.

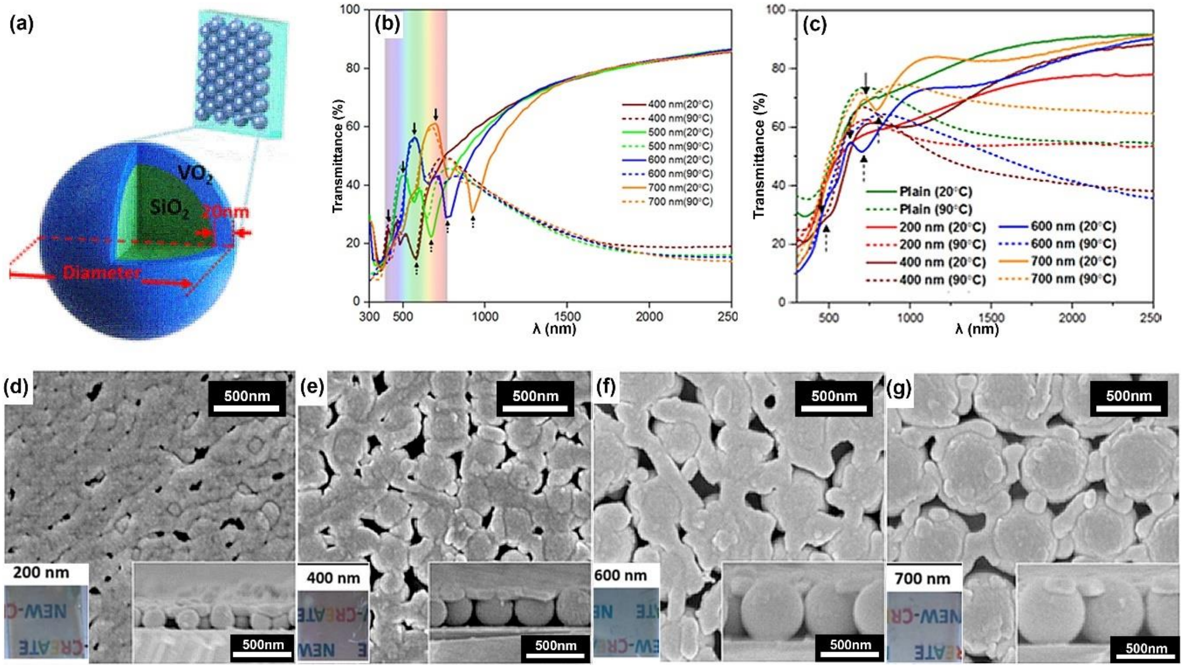

Figure 18 (a) Illustration of the two-dimensional $SiO_2$-$VO_2$ core-shell photonic structure on glass. (b) Calculated transmittance spectra of these structures with diameters of 400, 500, 600, and 700 nm, respectively. (c) measured transmittance spectra of the structures with silica sphere sizes of 200, 400, 600, and 700 nm, respectively, as well as the plain $VO_2$ film which serves as a control sample. The transmittance peaks and troughs are indicated by the solid and dashed arrows, respectively. (d-g) Top-view and (bottom-right insets) side-view SEM images of colour-changed samples using silica spheres with diameters of (d) 200, (e) 400, (f) 600, and (g) 700 nm, respectively and (inserted photographs on the bottom left) their corresponding normal-view appearance under sunlight. Adapted from Ref.[55] with permission. Copyright 2016 American Chemical Society.

# 3. Strategies used in CVD system for improving the energy storage performance of $VO_2$ film

## 3.1. Growth of core-shell structure

In 2014, Yin *et al.* produced $VO_2$ coated ZnO nanotetrapods via APCVD with the precursors of $VO(acac)_2$ and $N_2/O_2$ mixing gas (Figure 19) for field emission device applications[145]. The group employed ZnO as skeleton to overcome the difficulty of form $VO_2$ pure phase nanostructure due to its nonstandard vapour-liquid-solid (VLS) mechanism. The core-shell structure sample showed a temperature dependent field emission property, which had a higher field emission density with the temperature increasing and the temperature dependent property could be attributed to the $VO_2$ shell. The composite had a better field emission performance than $VO_2$ pure phase. This case is a good example of applying CVD to produce complex geometry composites and the idea of this case is useful for similar topic in future.

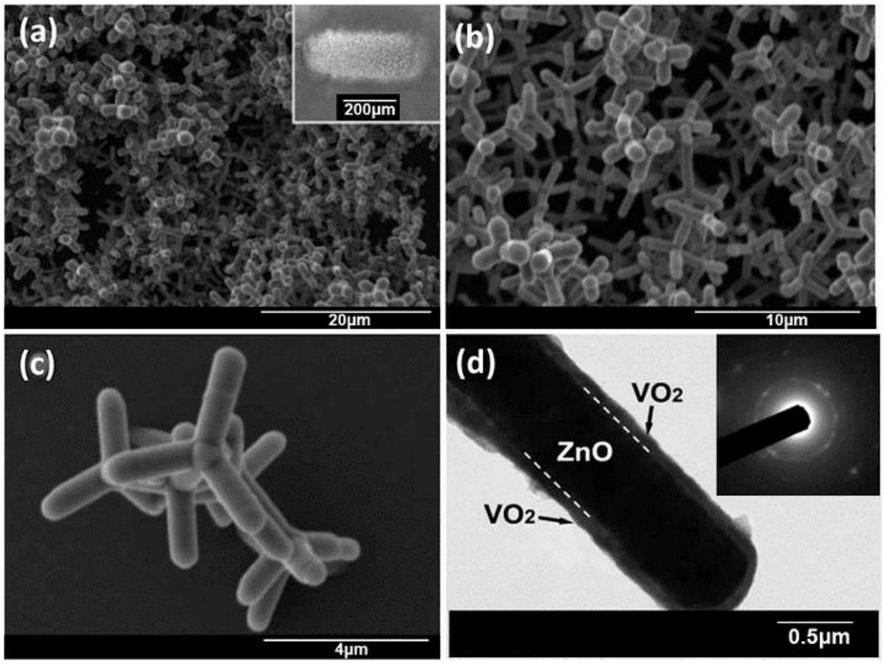

Figure 19 (a). low-, (b). medium-, and (c). high-magnification SEM images of $VO_2$-ZnO core-shell structure; (d) High-resolution transmission electron microscope (TEM) image of a single nanorod of a tetrapod; Upper inset in (d) is the corresponding SAED pattern. Adapted from Ref.[145] with permission from The Royal Society of Chemistry.

## 3.2. Morphology modification by changing growth parameter

Vernardou *et al.* deposited $VO_2$(B) films with different morphologies by controlling gas flow rate passing through precursor[146]. With an increase in the carrier gas flow rate, the film surface was smoothened, and the size of nanocrystal was decreased. The electrochemical properties of the film showed a negative relationship with the flow rate: the sample prepared with the lowest flow rate (1 L/min) had a specific discharge density of 425 mAh $g^{-1}$, with a capacitance retention of 97% after 500 cycles of charging (Figure 20). Porous thin films would allow easy access and wetting by the electrolyte which would increase the ion diffusion kinetics and improve the cycling stability, especially in supercapacitor electrodes. Utilizing the AACVD method, Warwick *et al.* synthesized highly porous $VO_2$(m) thin films and the crystallite size and porosity of the films can be controlled by varying the deposition time and electric field strength. The sample with small crystallite size, high porosity and best wetting properties displayed a specific capacitance of 3700 μF $cm^{-2}$ and stable cycling performance up to 1000 charge/discharge cycles[147].

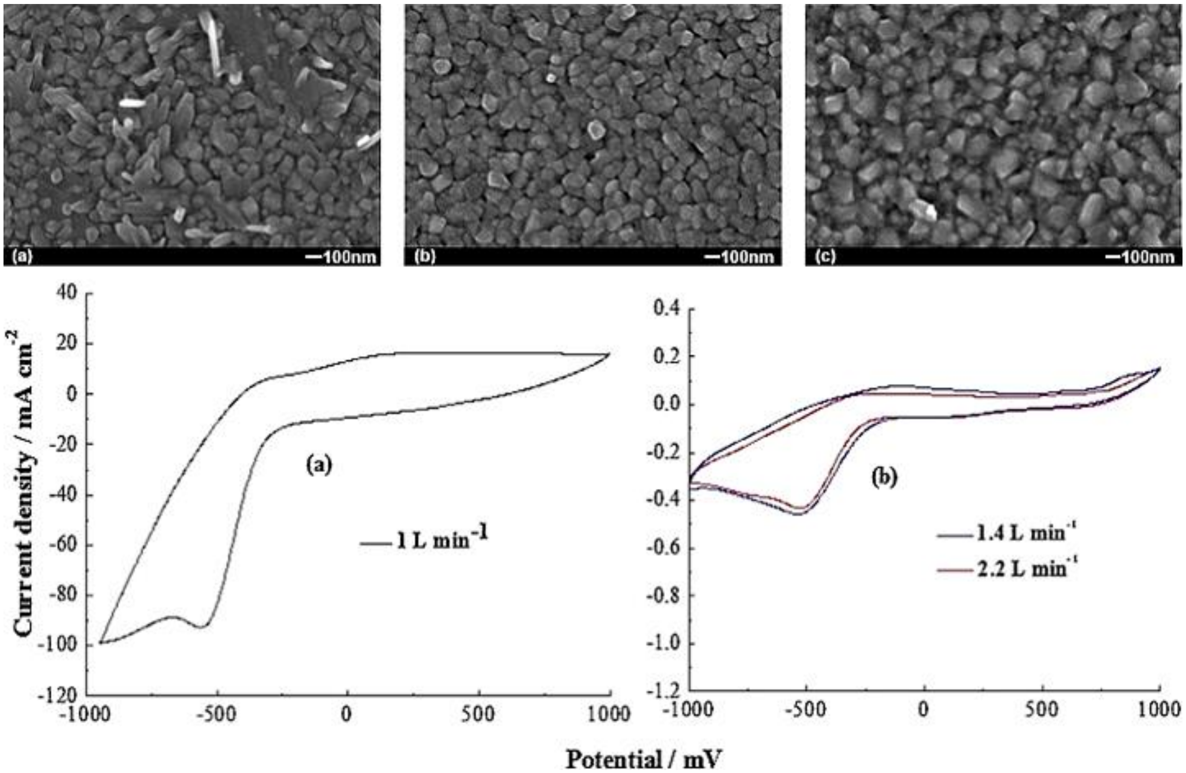

Figure 20 Field emission scanning electron microscope (FESEM) images and cyclic voltammograms of APCVD vanadium oxide coatings at 500 °C for a) 1; b) 1.4; and c) 2.2 L/min $N_2$ flow rate through the vanadium precursor bubbler. Reproduced from Ref.[146] with permission from Wiley.

### 3.3. Carbon/$VO_2$ heterostructure for battery and supercapacitor applications

Carbon/$VO_2$ heterostructures have drawn attentions as electrode materials for batteries and supercapacitors due to the combination of the good electrical conductivity of carbon and the high specific capacitance/lithium diffusion efficiency of $VO_2$. Rui *et al.* synthesised ultra-thin [approximate coating thickness ~4.3 nm, as shown in Figure 21 (d)] amorphous carbon coated $VO_2$

(B) belt via hydrothermal method for battery applications [Figure 21 (a)-(c)][148]. The ultra-thin carbon coating improved the electronic conductivity without blocking the lithium diffusion pathway. Compared with samples with different concentrations, the sample with 6.6wt% of carbon showed a balance between conductivity and lithium diffusion efficiency and the overall best charging rate capability compared to the other samples. Other heterostructure battery electrode materials that have been researched recently include graphene quantum dot coated $VO_2$ arrays[149] and $VO_2$(B) coated carbon fiber cloth[150]. Both materials showed good specific capacity, fast charging rate at high current density and excellent cycling durability. Moreover, the two structures showed more attractive properties such as flexibility and good compatibility for both Li-ion and Na-ion battery.

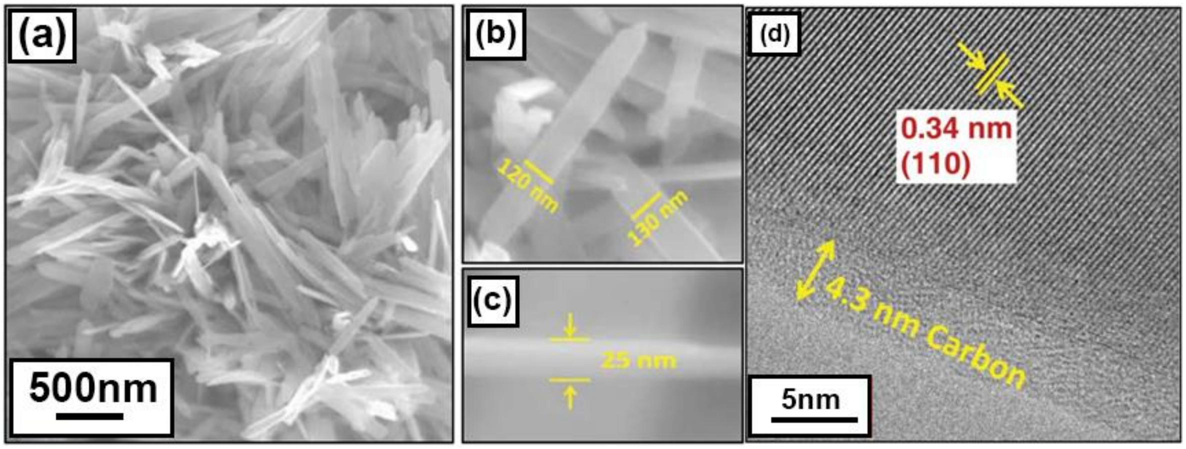

Figure 21 (a)-(c) SEM images and (d) TEM image of carbon/$VO_2$ (B) composite with 6.6wt% carbon content. Adapted from Ref.[148] with permission from The Royal Society of Chemistry.

On the other hand, heterostructures have also been intensively researched for supercapacitors. The structures for supercapacitor include graphene/$VO_2$(B) nanosheet composite hydrogel[151], $VO_x$ overcoated carbon nanotube (CNT) structure[152] and $VO_2$ nano-sphere decorated CNT heterostructure[153]. It is worth noting that researchers have employed CVD to produce $VO_x$ overcoating and $VO_2$ nanospheres, which proves CVD's capability for producing delicate nanoscale structures[153].

Table 5 summarised the strategies for improving the thermochromic and electrochemical performance discussed in the previous two chapters of the report, and the recommended CVD method for different strategies. As stated previously, APCVD is good at producing the high-quality thin film with accurate stoichiometry control and suitable for the applications required good covering and specified composition. AACVD and Hybrid AA/APCVD are suitable for mixing second phase into the matrix to produce composite materials. ALD is specialised in producing ultra-thin film with good quality.

Table 5 Strategies to improve the thermochromic and electrochemistry properties of $VO_2$ and the recommended CVD methods for applying the strategies.

| Applications | Strategy | Researching direction | Recommended CVD method | Purpose |
|---|---|---|---|---|
| To improve thermochromic performance | Doping | New element<br>Co-doping | APCVD | • To reduce $\tau_c$, enhance $\Delta T_{sol}$ and $T_{lum}$ in thermochromic materials |
| | Composite formation | Nanocomposite | AACVD, Hybrid AA/APCVD | |
| | | Mixed phase materials | AACVD | • Add multifunction such as photocatalytic to thermochromic materials |
| | | Multi-layered materials | APCVD, MOCVD, ALD | • Add multifunction such as hydrophobicity, photocatalytic and anti-oxidation ability to thermochromic film<br>• Enhance $\Delta T_{sol}$ and $T_{lum}$ at the same time |
| | Template-assisted growth | Biomimetic structure and<br>photonic crystal | APCVD, MOCVD, ALD | • Enhance both $T_{lum}$ and $\Delta T_{sol}$ and change colour and optical responses in thermochromic materials |
| To improve electrochemical performance | Composite formation | Ultra-thin carbon overcoating (~5nm) | ALD | • Enhance conductivity and lithium ion diffusivity to achieve maximum battery performance |
| | | Graphene quantum dot coated $VO_2$ arrays | ALD, APCVD | • Enhance conductivity, ion diffusivity and durability to achieve maximum battery performance<br>• Capable for both Li-ion and Na-ion battery |

| | | | | |
|---|---|---|---|---|
| | | $VO_2$(B) coated carbon fiber cloth | APCVD, MOCVD | • Balance conductivity, ion diffusivity and durability to achieve maximum battery performance<br>• Potential candidate for flexible Li-ion battery |
| | | $VO_x$ overcoated CNT structure<br>$VO_2$ nano-sphere decorated CNT | ALD, APCVD | • Balance conductivity, specific capacity and cycling durability to maximize supercapacitor performance |
| | Template-assisted growth | Core-shell structure | APCVD, MOCVD, ALD | • Enhance field emission properties |
| | Morphology controlling | Controlling crystalline grain size (from ~300 nm to ~100 nm) | APCVD, MOCVD | • Enhance discharge density and durability |
| | | Highly porous surface morphologies with extremely small surface features (~5 nm) | AACVD | • Enhance electrode/electrolyte interactions and improve cycling performance |

# 4. Conclusion and perspectives

## 4.1. Conclusion

This review discussed various CVD techniques and strategies to produce $VO_2$ polymorph thin films for energy storage and saving applications and their performances are largely determined by the crystallinity, phase and morphology. In the vanadium-oxygen system, the stoichiometry and the performance of the product are influenced by several parameters such as substrate temperature, the molar ratio of precursor and total flow rate. A ternary diagram and two 3D diagrams were plotted in relation to the phase and stoichiometry of thin film in APCVD system with vanadium halide precursor. The effects of processing condition on the film's quality in other CVD systems were discussed in detail. We reviewed some strategies to improve $VO_2$ thin film performance for both energy conservation and storage applications respectively. Three approaches, namely doping, composite forming, and template assisted growth to improve $VO_2$'s thermochromic performance further and add multifunction into the smart window system. Meanwhile, the electrochemical performance of $VO_2$ could be improved by forming core-shell structure material via template-assisted growth, modifying film morphology and forming carbon/$VO_2$ heterostructure. In summary, CVD is a promising technique to produce high quality and highly uniform $VO_2$ thin film with different morphology in large scale. This article can serve as a guideline for process control and performance enhancement in both energy conservation and storage applications.

## 4.2. Future research directions

Although $VO_2$ has been intensively researched for several years, there is still a long way to go before the commercialization and mass production of the final optimised product for thermochromic smart window and energy storage applications.

In the field of energy conservation, improving the thermochromic performance of $VO_2$ still remains a significant challenge. Currently $\tau_c$ at near room temperature can be achieved through doping and increasing $T_{lum}$ and $\Delta T_{sol}$ can be achieved through different methods such as nanopatterning, nanogridding and multi-layered materials. However, the three key requirements namely lower $\tau_c$ and enhanced $T_{lum}$ and $\Delta T_{sol}$ need to be improved simultaneously. Future research efforts should take this into consideration. Besides, multifunctional thermochromic device is vital for the next-generation energy conservation smart window. Lastly but most importantly, although $VO_2$ has been successfully deposited on large area, the batched production of VO2 based energy saving materials is currently still in exploration. The low-cost production of $VO_2$ based smart-window or window coating is highly sought after by both academia and industry, as they may hold great economic potential for commercialisation.

In the field of energy storage, current research is focussed on improving the electrochemical performance of $VO_2$ electrodes for battery and supercapacitor devices. In future studies, the electrochemical properties of $VO_2$ films can be enhanced with other metal oxides such as $Co_3O_4$ and $TiO_2$. Also, it is necessary to study and improve the electrochemical performance of $VO_2$ thick films, which are much needed for practical energy storage devices. Because of the abundant availability and low price of sodium (Na) and magnesium (Mg), Na-ion and Mg-ion batteries are currently attracting research attention. The applications of $VO_2$ in Na-ion and Mg-ion batteries would be an interesting topic for future research. Finally, the mass production of $VO_2$ based batteries and supercapacitors should be discussed in order to translate the $VO_2$ based product from the laboratory into our daily life.

Lastly, the current discussion of $VO_2$'s application in energy conservation and storage field is still mainly limited to material perspective and aims at the performance improvement of material. The discussion of $VO_2$ based device in energy perspective is relatively lacking. We suggest that more research can be conducted to focus on the actual impact of $VO_2$ on energy field such as the amount of energy saving in different region of the world; the optimised design of $VO_2$ coated smart window (for example the window size, installing location and window-to-wall ratio) for the best building energy saving effect; the contribution of $VO_2$ based energy storage device to the cost-cutting of electric vehicles; and the stability of the power grid after the introducing of $VO_2$ based battery or supercapacitor. The discussion based on the energy perspective will not only serve as a guideline for the material research to meet the real-world demand but also accelerate the applying of $VO_2$ based device in the actual applications.

## Acknowledgements

This research is supported by grants from the National Research Foundation, Prime Minister's Office, Singapore under its Campus of Research Excellence and Technological Enterprise (CREATE) programme, Ministry of Education (MOE) Tier one, RG124/16 and NRF2015NRF-POC002-019.

# References

[1] Omer AM. Energy, environment and sustainable development. Renewable Sustainable Energy Rev 2008;12:2265-300.

[2] Omer AM. Energy use and environmental impacts: A general review. J Renewable Sustainable Energy 2009;1:053101.

[3] Lemmet S. Buildings and climate change: Summary for decision-makers. Sustainable Buildings & Climate Initiative. Paris: United Nations Environmental Programme; 2009. p. 1-62.

[4] Yang L, Yan H, Lam JC. Thermal comfort and building energy consumption implications – A review. Appl Energy 2014;115:164-73.

[5] Kamalisarvestani M, Saidur R, Mekhilef S, Javadi FS. Performance, materials and coating technologies of thermochromic thin films on smart windows. Renewable Sustainable Energy Rev 2013;26:353-64.

[6] Cheung CK, Fuller RJ, Luther MB. Energy-efficient envelope design for high-rise apartments. Energy Build 2005;37:37-48.

[7] Synnefa A, Santamouris M, Akbari H. Estimating the effect of using cool coatings on energy loads and thermal comfort in residential buildings in various climatic conditions. Energy Build 2007;39:1167-74.

[8] Baetens R, Jelle BP, Gustavsen A. Properties, requirements and possibilities of smart windows for dynamic daylight and solar energy control in buildings: A state-of-the-art review. Sol Energy Mater Sol Cells 2010;94:87-105.

[9] Tarantini M, Loprieno AD, Porta PL. A life cycle approach to Green Public Procurement of building materials and elements: A case study on windows. Energy 2011;36:2473-82.

[10] Cocker TL, Titova LV, Fourmaux S, Holloway G, Bandulet HC, Brassard D, et al. Phase diagram of the ultrafast photoinduced insulator-metal transition in vanadium dioxide. Phys Rev B 2012;85:155120.

[11] Saeli M, Piccirillo C, Parkin IP, Binions R, Ridley I. Energy modelling studies of thermochromic glazing. Energy Build 2010;42:1666-73.

[12] Li S-Y, Niklasson GA, Granqvist CG. Thermochromic fenestration with $VO_2$-based materials: three challenges and how they can be met. Thin Solid Films 2012;520:3823-28.

[13] Liu C, Cao X, Kamyshny A, Law JY, Magdassi S, Long Y. $VO_2$/Si–Al gel nanocomposite thermochromic smart foils: largely enhanced luminous transmittance and solar modulation. J Colloid Interface Sci 2014;427:49-53.

[14] Li S-Y, Niklasson GA, Granqvist CG. Nanothermochromics with $VO_2$-based core-shell structures: calculated luminous and solar optical properties. J Appl Phys 2011;109:113515.

[15] Gao Y, Wang S, Kang L, Chen Z, Du J, Liu X, et al. $VO_2$-Sb:$SnO_2$ composite thermochromic smart glass foil. Energy Environ Sci 2012;5:8234-37.

[16] Kang L, Gao Y, Luo H, Chen Z, Du J, Zhang Z. Nanoporous thermochromic $VO_2$ films with low optical constants, enhanced luminous transmittance and thermochromic properties. ACS Appl Mater Interfaces 2011;3:135-38.

[17] Qian X, Wang N, Li Y, Zhang J, Xu Z, Long Y. Bioinspired multifunctional vanadium dioxide: improved thermochromism and hydrophobicity. Langmuir 2014;30:10766-71.

[18] Liu C, Wang N, Long Y. Multifunctional overcoats on vanadium dioxide thermochromic thin films with enhanced luminous transmission and solar modulation, hydrophobicity and anti-oxidation. Appl Surf Sci 2013;283:222-26.

[19] Liu C, Balin I, Magdassi S, Abdulhalim I, Long Y. Vanadium dioxide nanogrid films for high transparency smart architectural window applications. Opt Express 2015;23:A124-A32.

[20] Liu C, Long Y, Magdassi S, Mandler D. Ionic strength induced electrodeposition: a universal approach for nanomaterial deposition at selective areas. Nanoscale 2017;9:485-90.

[21] Lu Q, Liu C, Wang N, Magdassi S, Mandler D, Long Y. Periodic micro-patterned $VO_2$ thermochromic films by mesh printing. J Mater Chem C 2016;4:8385-91.

[22] Zhou Y, Cai Y, Hu X, Long Y. Temperature-responsive hydrogel with ultra-large solar modulation and high luminous transmission for "smart window" applications. J Mater Chem A 2014;2:13550-55.

[23] Zhou Y, Cai Y, Hu X, Long Y. $VO_2$/hydrogel hybrid nanothermochromic material with ultra-high solar modulation and luminous transmission. J Mater Chem A 2015;3:1121-26.

[24] Zhou Y, Layani M, Boey YCF, Sokolov I, Magdassi S, Long Y. Electro-thermochromic devices composed of self-assembled transparent electrodes and hydrogels. Adv Mater Technol 2016;1:1600069.

[25] Kumar S, Lenoble D, Maury F, Bahlawane N. Synthesis of vanadium oxide films with controlled morphologies: Impact on the metal–insulator transition behaviour. Phys Status Solidi A 2015;212:1582-87.

[26] Sahana MB, Dharmaprakash MS, Shivashankar SA. Microstructure and properties of $VO_2$ thin films deposited by MOCVD from vanadyl acetylacetonate. J Mater Chem 2002;12:333-38.

[27] Kang Y-B. Critical evaluation and thermodynamic optimization of the VO–$VO_{2.5}$ system. J Eur Ceram Soc 2012;32:3187-98.

[28] Bahlawane N, Lenoble D. Vanadium oxide compounds: structure, properties, and growth from the gas phase. Chem Vap Deposition 2014;20:299-311.

[29] Yan Y, Li B, Guo W, Pang H, Xue H. Vanadium based materials as electrode materials for high performance supercapacitors. J Power Sources 2016;329:148-69.

[30] Dunn B, Kamath H, Tarascon J-M. Electrical Energy Storage for the Grid: A Battery of Choices. Science 2011;334:928-35.

[31] Miller JR, Simon P. Electrochemical Capacitors for Energy Management. Science 2008;321:651-52.

[32] Simon P, Gogotsi Y, Dunn B. Where Do Batteries End and Supercapacitors Begin? Science 2014;343:1210-11.

[33] Köhler J, Makihara H, Uegaito H, Inoue H, Toki M. $LiV_3O_8$: characterization as anode material for an aqueous rechargeable Li-ion battery system. Electrochim Acta 2000;46:59-65.

[34] Murphy DW, Christian PA, DiSalvo FJ, Carides JN, Waszczak JV. Lithium incorporation by $V_6O_{13}$ and related vanadium (+4, +5) oxide cathode materials. J Electrochem Soc 1981;128:2053-60.

[35] Tsang C, Manthiram A. Synthesis of nanocrystalline $VO_2$ and its electrochemical behavior in lithium batteries. J Electrochem Soc 1997;144:520-24.

[36] Wu C, Xie Y. Promising vanadium oxide and hydroxide nanostructures: from energy storage to energy saving. Energy Environ Sci 2010;3:1191-206.

[37] Huynh WU, Dittmer JJ, Alivisatos AP. Hybrid nanorod-polymer solar cells. Science 2002;295:2425-27.

[38] Subba Reddy CV, Walker Jr EH, Wicker Sr SA, Williams QL, Kalluru RR. Synthesis of $VO_2$ (B) nanorods for Li battery application. Curr Appl Phys 2009;9:1195-98.

[39] Armstrong G, Canales J, Armstrong AR, Bruce PG. The synthesis and lithium intercalation electrochemistry of $VO_2$(B) ultra-thin nanowires. J Power Sources 2008;178:723-28.

[40] Liu J, Li Q, Wang T, Yu D, Li Y. Metastable vanadium dioxide nanobelts: hydrothermal synthesis, electrical transport, and magnetic properties. Angew Chem 2004;116:5158-62.

[41] Kannan AM, Manthiram A. Synthesis and electrochemical evaluation of high capacity nanostructured $VO_2$ cathodes. Solid State Ionics 2003;159:265-71.

[42] Liu H, Wang Y, Wang K, Hosono E, Zhou H. Design and synthesis of a novel nanothorn $VO_2$(B) hollow microsphere and their application in lithium-ion batteries. J Mater Chem 2009;19:2835-40.

[43] Zhang S, Li Y, Wu C, Zheng F, Xie Y. Novel flowerlike metastable vanadium dioxide (B) micronanostructures: facile synthesis and application in aqueous lithium ion batteries. J Phys Chem C 2009;113:15058-67.

[44] Jiang W, Ni J, Yu K, Zhu Z. Hydrothermal synthesis and electrochemical characterization of $VO_2$ (B) with controlled crystal structures. Appl Surf Sci 2011;257:3253-58.

[45] Luo JY, Xia YY. Aqueous lithium-ion battery $LiTi_2(PO_4)_3/LiMn_2O_4$ with high power and energy densities as well as superior cycling stability. Adv Funct Mater 2007;17:3877-84.

[46] Luo S, Tang Z, Lu J, Zhang Z. Electrochemical properties of carbon-mixed $LiFePO_4$ cathode material synthesized by the ceramic granulation method. Ceram Int 2008;34:1349-51.

[47] Wang F, Liu Y, Liu C-y. Hydrothermal synthesis of carbon/vanadium dioxide core–shell microspheres with good cycling performance in both organic and aqueous electrolytes. Electrochim Acta 2010;55:2662-66.

[48] Sun J, Chen Y, Priydarshi MK, Chen Z, Bachmatiuk A, Zou Z, et al. Direct chemical vapor deposition-derived graphene glasses targeting wide ranged applications. Nano Lett 2015;15:5846-54.

[49] Wang N, Huang Y, Magdassi S, Mandler D, Liu H, Long Y. Formation of $VO_2$ zero-dimensional/nanoporous layers with large supercooling effects and enhanced thermochromic properties. RSC Adv 2013;3:7124-28.

[50] Yue F, Huang W, Shi Q, Li D, Hu Y, Xiao Y, et al. Phase transition properties of vanadium oxide films deposited by polymer-assisted deposition. J Sol-Gel Sci Technol 2014;72:565-70.

[51] Du J, Gao Y, Luo H, Zhang Z, Kang L, Chen Z. Formation and metal-to-insulator transition properties of $VO_2$–$ZrV_2O_7$ composite films by polymer-assisted deposition. Sol Energy Mater Sol Cells 2011;95:1604-09.

[52] Wang N, Duchamp M, Xue C, Dunin-Borkowski RE, Liu G, Long Y. Single-crystalline W-doped $VO_2$ nanobeams with highly reversible electrical and plasmonic responses near room temperature. Adv Mater Interf 2016;3:1600164.

[53] Zhou J, Gao Y, Liu X, Chen Z, Dai L, Cao C, et al. Mg-doped $VO_2$ nanoparticles: hydrothermal synthesis, enhanced visible transmittance and decreased metal-insulator transition temperature. Phys Chem Chem Phys 2013;15:7505-11.

[54] Mjejri I, Etteyeb N, Sediri F. Mesoporous vanadium oxide nanostructures: hydrothermal synthesis, optical and electrochemical properties. Ceram Int 2014;40:1387-97.

[55] Ke Y, Balin I, Wang N, Lu Q, Tok LYA, White TJ, et al. Two-dimensional $SiO_2/VO_2$ photonic crystals with statically visible and dynamically infrared modulated for smart window deployment. ACS Appl Mater Interfaces 2016;8:33112-20.

[56] Zhang H-T, Zhang L, Mukherjee D, Zheng Y-X, Haislmaier RC, Alem N, et al. Wafer-scale growth of $VO_2$ thin films using a combinatorial approach. Nat Commun 2015;6:8475.

[57] Cao X, Thet MN, Zhang Y, Loo SCJ, Magdassi S, Yan Q, et al. Solution-based fabrication of $VO_2$ (M) nanoparticles via lyophilisation. RSC Adv 2015;5:25669-75.

[58] Lakes RS, Lee T, Bersie A, Wang YC. Extreme damping in composite materials with negative-stiffness inclusions. Nature 2001;410:565-67.

[59] Kim J, Ko C, Frenzel A, Ramanathan S, Hoffman JE. Nanoscale imaging and control of resistance switching in $VO_2$ at room temperature. Appl Phys Lett 2010;96:213106.

[60] Leroux C, Nihoul G, Van Tendeloo G. From $VO_2$(B) to $VO_2$(R): theoretical structures of $VO_2$ polymorphs and in situ electron microscopy. Phys Rev B 1998;57:5111-21.

[61] Warwick MEA, Binions R. Chemical vapour deposition of thermochromic vanadium dioxide thin films for energy efficient glazing. J Solid State Chem 2014;214:53-66.

[62] Jones AC, Hitchman ML. Chemical vapour deposition. [electronic resource] : precursors, processes and applications. Cambridge, UK: Royal Society of Chemistry; 2009.

[63] Dobkin DM, Zuraw MK. Principles of Chemical Vapor Deposition. [electronic resource]. Dordrecht: Springer Netherlands; 2003.

[64] MacChesney JB, Potter JF, Guggenheim HJ. Preparation and properties of vanadium dioxide films. J Electrochem Soc 1968;115:52-55.

[65] Vernardou D, Pemble ME, Sheel DW. The growth of thermochromic $VO_2$ films on glass by atmospheric-pressure CVD: a comparative study of precursors, CVD methodology, and substrates. Chem Vap Deposition 2006;12:263-74.

[66] Vernardou D, Paterakis P, Drosos H, Spanakis E, Povey IM, Pemble ME, et al. A study of the electrochemical performance of vanadium oxide thin films grown by atmospheric pressure chemical vapour deposition. Sol Energy Mater Sol Cells 2011;95:2842-47.

[67] Gaskell JM, Afzaal M, Sheel DW, Yates HM, Delfanazari K, Muskens OL. Optimised atmospheric pressure CVD of monoclinic $VO_2$ thin films with picosecond phase transition. Surf Coat Technol 2016;287:160-65.

[68] Manning TD, Parkin IP, Clark RJH, Sheel D, Pemble ME, Vernadou D. Intelligent window coatings: atmospheric pressure chemical vapour deposition of vanadium oxides. J Mater Chem 2002;12:2936-39.

[69] Wilkinson M, Kafizas A, Bawaked SM, Obaid AY, Al-Thabaiti SA, Basahel SN, et al. Combinatorial atmospheric pressure chemical vapor deposition of graded $TiO_2$–$VO_2$ mixed-phase composites and their dual functional property as self-cleaning and photochromic window coatings. ACS Comb Sci 2013;15:309-19.

[70] Manning TD, Parkin IP, Pemble ME, Sheel D, Vernardou D. Intelligent window coatings: atmospheric pressure chemical vapor deposition of tungsten-doped vnadium dioxide. Chem Mater 2004;16:744-49.

[71] Manning TD, Parkin IP. Vanadium(IV) oxide thin films on glass and silicon from the atmospheric pressure chemical vapour deposition reaction of $VOCl_3$ and water. Polyhedron 2004;23:3087-95.

[72] Kritikos L, Zambelis L, Papadimitropoulos G, Davazoglou D. Structure and electrical properties of selectively chemically vapor deposited vanadium oxide films from vanadium tri-i-propoxy oxide vapors. Surf Coat Technol 2007;201:9334-39.

[73] Louloudakis D, Vernardou D, Spanakis E, Katsarakis N, Koudoumas E. Thermochromic vanadium oxide coatings grown by APCVD at low temperatures. Phys Procedia 2013;46:137-41.

[74] Papadimitropoulos G, Kostis I, Trantalidis S, Tsiatouras A, Vasilopoulou M, Davazoglou D. Investigation of structural, morphological and electrical properties of APCVD vanadium oxide thin films. Phys Status Solidi C 2015;12:964-68.

[75] Vernardou D, Louloudakis D, Spanakis E, Katsarakis N, Koudoumas E. Thermochromic amorphous $VO_2$ coatings grown by APCVD using a single-precursor. Sol Energy Mater Sol Cells 2014;128:36-40.

[76] Maruyama T, Ikuta Y. Vanadium dioxide thin films prepared by chemical vapour deposition from vanadium(III) acetylacetonate. J Mater Sci 1993;28:5073-78.

[77] Spanò SF, Toro RG, Condorelli GG, Messina GML, Marletta G, Malandrino G. Phase-selective route to V-O film formation: a systematic MOCVD study into the effects of deposition temperature on structure and morphology Chem Vap Deposition 2015;21:319-26.

[78] Barreca D, Depero LE, Franzato E, Rizzi GA, Sangaletti L, Tondello E, et al. Vanadyl precursors psed to modify the properties of vanadium oxide thin flms obtained by chemical vapor deposition. J Electrochem Soc 1999;146:551-58.

[79] Vernardou D, Pemble ME, Sheel DW. Vanadium oxides prepared by liquid injection MOCVD using vanadyl acetylacetonate. Surf Coat Technol 2004;188–189:250-54.

[80] Barreca D, Armelao L, Caccavale F, Di Noto V, Gregori A, Rizzi GA, et al. Highly oriented $V_2O_5$ nanocrystalline thin films by plasma-enhanced chemical vapor deposition. Chem Mater 2000;12:98-103.

[81] Kuypers AD, Spee CIMA, Linden JL, Kirchner G, Forsyth JF, Mackor A. Plasma-enhanced CVD of electrochromic materials. Surf Coat Technol 1995;74:1033-37.

[82] Musschoot J, Deduytsche D, Poelman H, Haemers J, Van Meirhaeghe RL, Van den Berghe S, et al. Comparison of thermal and plasma-enhanced ALD/CVD of vanadium pentoxide. J Electrochem Soc 2009;156:122-26.

[83] Zhang JG, Liu P, Turner JA, Tracy CE, Benson DK. Highly stable vanadium oxide cathodes prepared by plasma-enhanced chemical vapor deposition. J Electrochem Soc 1998;145:1889-92.

[84] Marchand P, Hassan IA, Parkin IP, Carmalt CJ. Aerosol-assisted delivery of precursors for chemical vapour deposition: expanding the scope of CVD for materials fabrication. Dalton Trans 2013;42:9406-22.

[85] Naik AJT, Bowman C, Panjwani N, Warwick MEA, Binions R. Electric field assisted aerosol assisted chemical vapour deposition of nanostructured metal oxide thin films. Thin Solid Films 2013;544:452-56.

[86] Piccirillo C, Binions R, Parkin IP. Synthesis and functional properties of vanadium oxides: $V_2O_3$, $VO_2$, and $V_2O_5$ deposited on glass by aerosol-assisted CVD. Chem Vap Deposition 2007;13:145-51.

[87] Crane J, Warwick M, Smith R, Furlan N, Binions R. The application of electric fields to aerosol assisted chemical vapor deposition reactions. J Electrochem Soc 2011;158:D62-D67.

[88] Warwick MEA, Binions R. On the effects of electric fields in aerosol assisted chemical vapour deposition reactions of vanadyl acetylacetonate solutions in ethanol. J Nanosci Nanotechnol 2011;11:8126-31.

[89] Warwick MEA, Binions R. Electric field assisted aerosol assisted chemical vapor deposition of nanostructured metal oxide thin films. Surf Coat Technol 2013;230:28-32.

[90] Warwick MEA, Ridley I, Binions R. Electric fields in the chemical vapour deposition growth of vanadium dioxide thin films. J Nanosci Nanotechnol 2011;11:8158-62.

[91] Warwick MEA, Ridley I, Binions R. Thermochromic vanadium dioxide thin films from electric field assisted aerosol assisted chemical vapour deposition. Surf Coat Technol 2013;230:163-67.

[92] Warwick MEA, Ridley I, Binions R. Thermochromic vanadium dioxide thin films prepared by electric field assisted atmospheric pressure chemical vapour deposition for intelligent glazing application and their energy demand reduction properties. Sol Energy Mater Sol Cells 2016;157:686-94.

[93] Warwick MEA, Binions R. Thermochromic vanadium dioxide thin films from electric field assisted aerosol assisted chemical vapour deposition. Sol Energy Mater Sol Cells 2015;143:592-600.

[94] Warwick MEA, Dunnill CW, Goodall J, Darr JA, Binions R. Hybrid chemical vapour and nanoceramic aerosol assisted deposition for multifunctional nanocomposite thin films. Thin Solid Films 2011;519:5942-48.

[95] Blanquart T, Niinisto J, Gavagnin M, Longo V, Heikkila M, Puukilainen E, et al. Atomic layer deposition and characterization of vanadium oxide thin films. RSC Advances 2013;3:1179-85.

[96] Premkumar PA, Martens K, Rampelberg G, Toeller M, Ablett JM, Meersschaut J, et al. Metal-insulator transition in ALD $VO_2$ ultrathin films and nanoparticles: morphological control. Adv Funct Mater 2015;25:679-86.

[97] Premkumar PA, Toeller M, Radu IP, Adelmann C, Schaekers M, Meersschaut J, et al. Process study and characterization of $VO_2$ thin films synthesized by ALD using TEMAV and $O_3$ precursors. ECS J Solid State Sci Technol 2012;1:P169-P74.

[98] Tangirala M, Zhang K, Nminibapiel D, Pallem V, Dussarrat C, Cao W, et al. Physical analysis of $VO_2$ films grown by atomic layer deposition and RF magnetron sputtering. ECS J Solid State Sci Technol 2014;3:N89-N94.

[99] Rampelberg G, Schaekers M, Martens K, Xie Q, Deduytsche D, Schutter BD, et al. Semiconductor-metal transition in thin $VO_2$ films grown by ozone based atomic layer deposition. Appl Phys Lett 2011;98:162902.

[100] Kim C-Y, Kim SH, Kim SJ, An K-S. $VO_2$(1 1 0) film formation on $TiO_2$(1 1 0) through post-reduction of ALD grown vanadium oxide. Appl Surf Sci 2014;313:368-71.

[101] Dagur P, Mane AU, Shivashankar SA. Thin films of $VO_2$ on glass by atomic layer deposition: microstructure and electrical properties. J Cryst Growth 2005;275:e1223-e28.

[102] Chen X, Pomerantseva E, Banerjee P, Gregorczyk K, Ghodssi R, Rubloff G. Ozone-based atomic layer deposition of crystalline $V_2O_5$ films for high performance electrochemical energy storage. Chem Mater 2012;24:1255-61.

[103] Musschoot J, Deduytsche D, Van Meirhaeghe RL, Detavernier C. ALD of vanadium oxide. ECS Trans 2009;25:29-37.

[104] Suntola T. Atomic layer epitaxy. Mater Sci Rep 1989;4:261-312.

[105] Romanyuk A, Steiner R, Marot L, Oelhafen P. Temperature-induced metal–semiconductor transition in W-doped $VO_2$ films studied by photoelectron spectroscopy. Sol Energy Mater Sol Cells 2007;91:1831-35.

[106] Blackman CS, Piccirillo C, Binions R, Parkin IP. Atmospheric pressure chemical vapour deposition of thermochromic tungsten doped vanadium dioxide thin films for use in architectural glazing. Thin Solid Films 2009;517:4565-70.

[107] Manning TD, Parkin IP. Atmospheric pressure chemical vapour deposition of tungsten doped vanadium(iv) oxide from $VOCl_3$, water and $WCl_6$. J Mater Chem 2004;14:2554-59.

[108] Binions R, Hyett G, Piccirillo C, Parkin IP. Doped and un-doped vanadium dioxide thin films prepared by atmospheric pressure chemical vapour deposition from vanadyl acetylacetonate and tungsten hexachloride: the effects of thickness and crystallographic orientation on thermochromic properties. J Mater Chem 2007;17:4652-60.

[109] Binions R, Piccirillo C, Palgrave RG, Parkin IP. Hybrid aerosol assisted and atmospheric pressure CVD of gold-doped vanadium dioxide. Chem Vap Deposition 2008;14:33-39.

[110] Vernardou D, Pemble ME, Sheel DW. Tungsten-doped vanadium oxides prepared by direct liquid injection MOCVD. Chem Vap Deposition 2007;13:158-62.

[111] Piccirillo C, Binions R, Parkin IP. Nb-doped $VO_2$ thin films prepared by aerosol-assisted chemical vapour deposition. Eur J Inorg Chem 2007;2007:4050-55.

[112] Burkhardt W, Christmann T, Meyer BK, Niessner W, Schalch D, Scharmann A. W- and F-doped $VO_2$ films studied by photoelectron spectrometry. Thin Solid Films 1999;345:229-35.

[113] Kiri P, Warwick MEA, Ridley I, Binions R. Fluorine doped vanadium dioxide thin films for smart windows. Thin Solid Films 2011;520:1363-66.

[114] Manning TD, Parkin IP, Blackman C, Qureshi U. APCVD of thermochromic vanadium dioxide thin films-solid solutions $V_{2-x}M_xO_2$ (M = Mo, Nb) or composites $VO_2$ : $SnO_2$. J Mater Chem 2005;15:4560-66.

[115] Burkhardt W, Christmann T, Franke S, Kriegseis W, Meister D, Meyer BK, et al. Tungsten and fluorine co-doping of $VO_2$ films. Thin Solid Films 2002;402:226-31.

[116] Binions R, Piccirillo C, Parkin IP. Tungsten doped vanadium dioxide thin films prepared by atmospheric pressure chemical vapour deposition from vanadyl acetylacetonate and tungsten hexachloride. Surf Coat Technol 2007;201:9369–72.

[117] Chen S, Dai L, Liu J, Gao Y, Liu X, Chen Z, et al. The visible transmittance and solar modulation ability of $VO_2$ flexible foils simultaneously improved by Ti doping: an optimization and first principle study. Phys Chem Chem Phys 2013;15:17537-43.

[118] Du J, Gao Y, Luo H, Kang L, Zhang Z, Chen Z, et al. Significant changes in phase-transition hysteresis for Ti-doped $VO_2$ films prepared by polymer-assisted deposition. Sol Energy Mater Sol Cells 2011;95:469-75.

[119] Wang N, Liu S, Zeng XT, Magdassi S, Long Y. Mg/W-codoped vanadium dioxide thin films with enhanced visible transmittance and low phase transition temperature. J Mater Chem C 2015;3:6771-77.

[120] Batista C, Ribeiro RM, Teixeira V. Synthesis and characterization of $VO_2$-based thermochromic thin films for energy-efficient windows. Nanoscale Res Lett 2011;6:301.

[121] Greenberg CB. Undoped and doped $VO_2$ films grown from $VO(OC_3H_7)_3$. Thin Solid Films 1983;110:73-82.

[122] Béteille F, Livage J. Optical switching in $VO_2$ thin films. J Sol-Gel Sci Technol 1998;13:915-21.

[123] Lee M-H, Kim M-G, Song H-K. Thermochromism of rapid thermal annealed $VO_2$ and Sn-doped $VO_2$ thin films. Thin Solid Films 1996;290–291:30-33.

[124] Chen B, Yang D, Charpentier PA, Zeman M. $Al^{3+}$-doped vanadium dioxide thin films deposited by PLD. Sol Energy Mater Sol Cells 2009;93:1550-54.

[125] Phillips TE, Murphy RA, Poehler TO. Electrical studies of reactively sputtered Fe-doped $VO_2$ thin films. Mater Res Bull 1987;22:1113-23.

[126] Song L, Zhang Y, Huang W, Shi Q, Li D, Zhang Y, et al. Preparation and thermochromic properties of Ce-doped $VO_2$ films. Mater Res Bull 2013;48:2268-71.

[127] Ufert KD. Doping of $VO_2$ thin films by ion implantation. Phys Status Solidi A 1977;42:187-90.

[128] Gao Y, Cao C, Dai L, Luo H, Kanehira M, Ding Y, et al. Phase and shape controlled $VO_2$ nanostructures by antimony doping. Energy Environ Sci 2012;5:8708-15.

[129] Wang N, Duchamp M, Dunin-Borkowski RE, Liu S, Zeng X, Cao X, et al. Terbium-doped $VO_2$ thin films: reduced phase transition temperature and largely enhanced luminous transmittance. Langmuir 2016;32:759-64.

[130] Wang N, Chew Shun NT, Duchamp M, Dunin-Borkowski RE, Li Z, Long Y. Effect of lanthanum doping on modulating the thermochromic properties of $VO_2$ thin films. RSC Adv 2016;6:48455-61.

[131] Cao X, Wang N, Magdassi S, Mandler D, Long Y. Europium doped vanadium dioxide material: reduced phase transition temperature, enhanced luminous transmittance and solar modulation. Sci Adv Mater 2014;6:558-61.

[132] Mlyuka NR, Niklasson GA, Granqvist CG. Mg doping of thermochromic $VO_2$ films enhances the optical transmittance and decreases the metal-insulator transition temperature. Appl Phys Lett 2009;95:171909.

[133] Li S-Y, Niklasson GA, Granqvist CG. Nanothermochromics: calculations for $VO_2$ nanoparticles in dielectric hosts show much improved luminous transmittance and solar energy transmittance modulation. J Appl Phys 2010;108:063525.

[134] Li S-Y, Mlyuka NR, Primetzhofer D, Hallén A, Possnert G, Niklasson GA, et al. Bandgap widening in thermochromic Mg-doped $VO_2$ thin films: quantitative data based on optical absorption. Appl Phys Lett 2013;103:161907.

[135] Shen N, Chen S, Chen Z, Liu X, Cao C, Dong B, et al. The synthesis and performance of Zr-doped and W-Zr-codoped $VO_2$ nanoparticles and derived flexible foils. J Mater Chem A 2014;2:15087-93.

[136] Wang N, Goh QS, Lee PL, Magdassi S, Long Y. One-step hydrothermal synthesis of rare earth/W-codoped $VO_2$ nanoparticles: Reduced phase transition temperature and improved thermochromic properties. J Alloys Compd 2017;711:222-28.

[137] Saeli M, Piccirillo C, Parkin IP, Ridley I, Binions R. Nano-composite thermochromic thin films and their application in energy-efficient glazing. Sol Energy Mater Sol Cells 2010;94:141-51.

[138] Saeli M, Binions R, Piccirillo C, Hyett G, Parkin IP. Templated growth of smart nanocomposite thin films: Hybrid aerosol assisted and atmospheric pressure chemical vapour deposition of vanadyl acetylacetonate, auric acid and tetraoctyl ammonium bromide. Polyhedron 2009;28:2233-39.

[139] Qureshi U, Manning TD, Parkin IP. Atmospheric pressure chemical vapour deposition of $VO_2$ and $VO_2/TiO_2$ films from the reaction of $VOCl_3$, $TiCl_4$ and water. J Mater Chem 2004;14:1190-94.

[140] Qureshi U, Manning TD, Blackman C, Parkin IP. Composite thermochromic thin films: ($TiO_2$)–($VO_2$) prepared from titanium isopropoxide, $VOCl_3$ and water. Polyhedron 2006;25:334-38.

[141] Evans P, Pemble ME, Sheel DW, Yates HM. Multi-functional self-cleaning thermochromic films by atmospheric pressure chemical vapour deposition. J Photochem Photobiol, A 2007;189:387-97.

[142] Breckenfeld E, Kim H, Burgess K, Charipar N, Cheng SF, Stroud R, et al. Strain effects in epitaxial $VO_2$ thin films on columnar buffer-layer $TiO_2$/$Al_2O_3$ virtual substrates. ACS Appl Mater Interfaces 2017;9:1577-84.

[143] Taylor A, Parkin I, Noor N, Tummeltshammer C, Brown MS, Papakonstantinou I. A bioinspired solution for spectrally selective thermochromic $VO_2$ coated intelligent glazing. Opt Express 2013;21:A750-A64.

[144] Ke Y, Wen X, Zhao D, Che R, Xiong Q, Long Y. Controllable fabrication of two-dimensional patterned $VO_2$ nanoparticle, nanodome, and nanonet arrays with tunable temperature-dependent localized surface plasmon resonance. ACS Nano 2017.

[145] Yin H, Yu K, Song C, Wang Z, Zhu Z. Low-temperature CVD synthesis of patterned core-shell $VO_2$@ZnO nanotetrapods and enhanced temperature-dependent field-emission properties. Nanoscale 2014;6:11820-27.

[146] Vernardou D, Apostolopoulou M, Louloudakis D, Katsarakis N, Koudoumas E. Electrochemical performance of vanadium oxide coatings grown using atmospheric pressure CVD. Chem Vap Deposition 2015;21:369-74.

[147] Warwick MEA, Roberts AJ, Slade RCT, Binions R. Electric field assisted chemical vapour deposition - a new method for the preparation of highly porous supercapacitor electrodes. J Mater Chem A 2014;2:6115-20.

[148] Rui X, Sim D, Xu C, Liu W, Tan H, Wong K, et al. One-pot synthesis of carbon-coated $VO_2$(B) nanobelts for high-rate lithium storage. RSC Adv 2012;2:1174-80.

[149] Chao D, Zhu C, Xia X, Liu J, Zhang X, Wang J, et al. Graphene quantum dots coated $VO_2$ arrays for highly durable electrodes for Li and Na ion batteries. Nano Lett 2015;15:565-73.

[150] Li S, Liu G, Liu J, Lu Y, Yang Q, Yang L-Y, et al. Carbon fiber cloth@$VO_2$ (B): excellent binder-free flexible electrodes with ultrahigh mass-loading. J Mater Chem A 2016;4:6426-32.

[151] Wang H, Yi H, Chen X, Wang X. One-step strategy to three-dimensional graphene/$VO_2$ nanobelt composite hydrogels for high performance supercapacitors. J Mater Chem A 2014;2:1165-73.

[152] Boukhalfa S, Evanoff K, Yushin G. Atomic layer deposition of vanadium oxide on carbon nanotubes for high-power supercapacitor electrodes. Energy Environ Sci 2012;5:6872-79.

[153] Jampani PH, Kadakia K, Hong DH, Epur R, Poston JA, Manivannan A, et al. CVD derived vanadium oxide nano-sphere-carbon nanotube (CNT) nano-composite hetero-structures: high energy supercapacitors. J Electrochem Soc 2013;160:A1118-A27.